NASA TECHNICAL MEMORANDUM

NASA TM X-1657

NASA TM X-1657

PERFORMANCE OF A COLLAPSIBLE PLUG NOZZLE HAVING EITHER TWO-POSITION CYLINDRICAL OR VARIABLE ANGLE FLOATING SHROUDS AT MACH NUMBERS FROM 0 TO 2.0

by Robert A. Wasko and Douglas E. Harrington

Lewis Research Center
Cleveland, Ohio

NATIONAL AERONAUTICS AND SPACE ADMINISTRATION • WASHINGTON, D. C. • OCTOBER 1968

NASA TM X-1657

PERFORMANCE OF A COLLAPSIBLE PLUG NOZZLE HAVING EITHER TWO-POSITION CYLINDRICAL OR VARIABLE ANGLE FLOATING SHROUDS AT MACH NUMBERS FROM 0 TO 2.0

By Robert A. Wasko and Douglas E. Harrington

Lewis Research Center
Cleveland, Ohio

NATIONAL AERONAUTICS AND SPACE ADMINISTRATION

For sale by the Clearinghouse for Federal Scientific and Technical Information
Springfield, Virginia 22151 – CFSTI price $3.00

ABSTRACT

An experimental study was made concerning the effects of two types of shroud geometry on the performance of a collapsible plug nozzle. Shroud geometries considered were a two-position cylindrical shroud and a variable angle floating shroud. Quiescent performance was obtained at nozzle pressure ratios from 2 to 15, and external flow effects were obtained at Mach numbers from 0.56 to 1.97. At subsonic cruise, the performance of the two-position shroud was nearly comparable to that of the floating shroud. However, the two-position shroud had better performance for subsonic acceleration whereas the floating shroud had better performance at supersonic Mach numbers. Maximum external flow effects occurred at Mach 1.2 for both shroud configurations.

PERFORMANCE OF A COLLAPSIBLE PLUG NOZZLE HAVING EITHER TWO-POSITION CYLINDRICAL OR VARIABLE ANGLE FLOATING SHROUDS AT MACH NUMBERS FROM 0 TO 2.0

Lewis Research Center

SUMMARY

An experimental study was made concerning the effects of two types of shroud geometry on the performance of a collapsible plug nozzle. Shroud geometries considered were a two-position cylindrical shroud and a variable angle floating shroud. Quiescent performance was obtained at nozzle pressure ratios from 2 to 15, and external flow effects were obtained at Mach numbers from 0.56 to 1.97. The nozzle performance for the two-position shroud and floating shroud were nearly comparable at subsonic cruise. For example, the nozzle efficiency at the Mach 0.85 cruise point was 0.932 for the two-position shroud and 0.930 for the floating shroud. However, the two-position shroud had better performance at supersonic Mach numbers. The nozzle efficiencies of the two-position and floating shroud, respectively, were 0.959 and 0.943 at Mach 0.56, and 0.928 and 0.948 at Mach 1.97. Maximum external flow effects occurred at Mach 1.2 for both shroud configurations where a performance loss of 5.1 percent of ideal thrust was observed for the two-position shroud and 5.8 percent for the floating shroud.
shroud and 5.8 percent for the floating shroud.

INTRODUCTION

Multimission jet aircraft put stringent demands on the exhaust nozzle system. This type of aircraft is designed primarily for subsonic cruise but has supersonic dash and limited supersonic cruise capabilities. As part of a broad program in airbreathing propulsion, the Lewis Research Center is evaluating various nozzle geometries appropriate for application to both supersonic cruise and multimission aircraft. In this continuing program, plug nozzles are receiving considerable emphasis because they offer the potential of good aerodynamic performance and they may also provide suppression of infrared radiation from internal hardware. For multimission aircraft, the plug nozzle may take

the form of a low-angle conical plug nozzle with a sonic discharge for optimum subsonic cruise performance. Performance is optimized for supersonic dash and cruise by variable shroud geometry that provides internal expansion appropriate to the flight conditions. Two variable shroud concepts of this type are a translating shroud and a floating shroud. The floating shroud is aerodynamically actuated to an exit area fixed by a balance of pressure forces on the internal and external surface of the shroud. The translating shroud is mechanically extended to provide internal expansion. The nozzle design must also include the capability for throat area variation due to afterburner operation. One concept for achieving this with a plug nozzle is to collapse a portion of the plug surface.

This report presents results of an experimental study concerning the effects of two types of shroud geometry on the off-design performance of a collapsible plug nozzle. Shroud geometries considered were a cylindrical, two-position shroud, and a variable angle floating shroud. The two-position shroud could be fully retracted, resulting in a sonic discharge, or extended to provide a maximum internal area ratio of 2.13. The floating shroud provided internal expansion that varied with nozzle pressure ratio between mechanical stops that permitted a minimum area ratio of 1.05 and a maximum of 2.56 Three fixed geometries of the centerbody were tested which simulated positions of a collapsible plug corresponding to a full reheat condition, partial reheat, and no reheat. Cold-flow models were tested for internal performance in a quiescent test facility of the Lewis Research Center, at nozzle pressure ratios from 2 to 15. External flow effects were obtained in the transonic test section of the 8- by 6-Foot Supersonic Wind Tunnel at Mach numbers from 0.56 to 1.97.

SYMBOLS

$A_{Boattail}$	projected boattail area, in.^{2} (cm^2)
A_9	annular area at nozzle exit, in.^{2} (cm^2)
A^*	nozzle throat area, in.^{2} (cm^2)
C_{D8}	nozzle discharge coefficient
d	model diameter, in. (cm)
F	measured nozzle thrust, or nozzle thrust-minus-drag
F_i	ideal nozzle thrust
$\Delta(F/F_i)$	loss in performance due to external flow effects
l	plug length measured from throat station, in. (cm)
M_l	local Mach number

M_0	free-stream Mach number
max	maximum
min	minimum
P_7	nozzle total pressure
$\bar{P}_7$	average nozzle total pressure
p_l	local plug static pressure
p_0	free-stream static pressure
r	internal model radius, in. (cm)
x	axial distance from throat station, in. (cm)
y	radial distance in plane of total pressure rake, in. (cm)
β	boattail angle, deg

APPARATUS AND PROCEDURE

Quiescent Test

Quiescent performance was obtained in a test chamber connected to the supply air and exhaust system facilities of the Lewis Research Center, as shown in figures 1 and 2. Nozzle pressure ratio was varied by maintaining a constant air-supply pressure and varying the test chamber static pressure. The average total pressure in the model was determined from a rake.

The actual weight flow rate was computed from the average total pressure and temperature measurements at the weight flow measuring station (fig. 2) and a calibration constant for the flow system based on measurements for ASME nozzles. Nozzle ideal weight flow was calculated from measured nozzle total pressure and temperature, and the choked throat area. Nozzle discharge coefficient was calculated from the ratio of measured-to-ideal weight flow.

Test nozzles were attached to a mounting pipe, which was supported on a bed plate, and freely suspended in the test chamber by flexure rods. The bed plate was connected to a load cell through a beam linkage. The load cell was a pressure diaphragm type and was calibrated by static weights. The load cell force is a result of all the forces acting on the flow system: the nozzle force, flow momentum at the bellmouth inlet, and the resistance force on the pipe at the labyrinth seals. Therefore, the nozzle force was calculated from the algebraic sum of the inlet momentum, labyrinth seal pressure force, and the load cell output. The labyrinth seals separate the supply air from the altitude exhaust and provide a means of maintaining a pressure difference across the nozzle. The laby-

rinth seal pressure force and the inlet momentum were obtained from facility calibrations.

External Flow Test

Nozzle performance with external flow was obtained in the 8- by 6-Foot Supersonic Wind Tunnel. The model installation is shown in figures 3 and 4. The model external shell was grounded and was supported from the tunnel ceiling by a hollow, vertical strut. The nozzle-adapter portion of the model was attached to the air bottle, which was cantilevered by flow tubes from supply manifolds located outside the test section. Front and rear bearings supported the air bottle. The plug was attached to the shroud by struts; thus, the nozzle axial force (thrust-minus-drag) was transmitted to the load cell in the nose of the model shell. The most forward part of the nozzle section was arbitrarily defined as a point 0.75 model diameters upstream of the nominal throat station. The adapter section was defined as the remaining portion of the afterbody. Since the floating part of the model included both the adapter section and nozzle section, the measured axial force represented the thrust-minus-drag of the adapter and nozzle section. The nozzle thrust-minus-drag was calculated from the sum of the measured axial force and the calculated friction drag of the adapter section. Friction drag on the adapter section was estimated using the semi-empirical, flat plate, mean skin friction coefficient given in figure 7 of reference 1 as a function of free-stream Mach number and Reynolds number. The coefficient accounts for variations in boundary layer thickness and flow profile with Reynolds number. Previous measurements of the boundary-layer characteristics at the aft end of this jet exit model in the 8- by 6-Foot Supersonic Wind Tunnel indicated that the profile and thickness were essentially the same as that computed for a flat plate of equal length. The strut wake appeared to affect only a localized region near the top of the model and resulted in a slightly lower local free-stream velocity than measured on the side and bottom of the model. Therefore, the results of reference 1 were used without correction for three-dimensional flow effects or strut interference effects.

A static calibration of the thrust measuring system was obtained by applying a known force to the nozzle and measuring the output of the load cell. To minimize changes in the calibration due to variations in temperature (e. g., aerodynamic heating due to external flow), the load cell was surrounded by a water-cooled jacket and was maintained at a constant temperature.

Nozzle weight flow was determined from continuity, average rake total pressure, total temperature measured in the air bottle, and the nozzle discharge coefficient determined from the quiescent test. Table I lists the discharge coefficients for all configurations tested.

The ambient pressure is constant for a given free-stream Mach number; thus, a

variation in nozzle pressure ratio was obtained by varying the internal total pressure.

Nozzle Geometry and Instrumentation

Two-position shroud. - Details of the two-position shroud are shown in figure 5(a). Cylindrical shrouds with fixed shroud extenstions were used to simulate a mechanically-actuated two-position shroud. These shrouds were slip-fitted over the 8.5-inch (22.16-cm) nozzle afterbody. Shroud extension was measured relative to the nominal throat station. For the retracted shroud geometry, the shroud tip was upstream of the nominal throat and the nozzle had a sonic discharge for all plugs tested. For the extended shroud geometry, the shroud tip extended 3.02 inches (7.67 cm) downstream of the nominal throat. This is equivalent to an extension ratio of 0.355 based on the 8.5-inch (22.16-cm) body diameter. This extension results in internal expansion having area ratios (A_9/A^*) of 1.31, 1.60, and 2.13 for the full (maximum) reheat plug, partial (part) reheat plug, and no-reheat (cruise) plug, respectively. These area ratios are listed in table I as well as the corresponding nozzle pressure ratios based on one-dimensional, isentropic expansion of the flow to ambient pressure at the nozzle exit (P_7/p_0). The angle (β) of the boattail surface on the shroud (external boattail) was 8°. The internal boattail, also 8°, is related to the inclination angle of the throat. The boattail area projected in the axial direction is listed in table I.

Floating shroud. - The floating shroud geometry is shown in figure 5(b). The floating shroud was made on interconnected flaps and seals and was 3.743 inches (9.52 cm) long. The flaps and seals were attached to a ring that formed a pin hinge at the nominal throat station. The minimum and maximum exit area for each plug shown in table I result from minimum and maximum shroud travel limits. The values of A_9/A^*, P_7/p_0, $A_{Boattail}$, and β correspond to these minimum and maximum exit areas. The maximum stop was such that the shroud could expand greater than the afterbody diameter, resulting in negative boattail angles. The floating shroud in a flared position is shown in figure 3. The shroud was limited to boattail angles of $11^\circ \geq \beta \geq -3.3^\circ$. The minimum stop limited the exit area such that A_9/A^* was never less than 1.05. During initial quiescent tests of the floating shroud nozzle, the minimum exit area was not limited as mentioned, and the nozzle was found to be unstable for the cruise configuration at nozzle pressure ratios from 2.9 to 3.8 and for the part-reheat configurations at pressure ratios less than 4.5. A severe flutter occurred for the part-reheat configuration, which resulted in a model failure and precluded testing of the maximum-reheat configuration. The unstable regimes were analyzed and it was concluded that the aerodynamic flutter occurred due to sonic point travel between the throat and nozzle exit. Aerodynamic flutter did not occur

during subsequent quiescent testing of the floating shroud nozzles having stops that limited the minimum exit area.

Plugs. - Details of plug geometry are presented in figure 6. The fixed geometries tested simulated a maximum-to-minimum throat area variation of 2.03. The cruise plug, shown in figure 6(a), was a 10° half-angle cone to a point just inside the nozzle exit. The plug throat section is defined for the purpose of plug pressure distributions. These will be presented in a later figure as a function of distance downstream of the plug throat station. The corresponding location of the sonic point on the plug is not implied to occur at the same axial station.

The part-reheat plug (fig. 6(b)) consists of a 10° half-angle cone up to the hinge point and a 6.7° half-angle conic section up to the plug throat station. The hinge point would separate the collapsible and stationary parts of the plug in actual hardware.

The maximum-reheat plug (fig. 6(c)) consists of a 10° half-angle cone up to the hinge point and a 3.15° half-angle conic section up to the plug throat station. The plug surface irregularities inside the nozzle result from mechanical details assumed to exist in the collapsible hardware.

Instrumentation. - Typical plug static pressure instrumentation is shown in figure 7. Although the cruise plug is shown, orifice numbers are common to all plugs. Orifices are located by the distance (x) downstream of the plug throat station. The plug length (ℓ) is also measured in this manner. Table II lists the orifice location for each plug as well as a nondimensional position coordinate (x/ℓ).

Rake instrumentation, used for determining nozzle total pressure, was located as shown schematically in figure 8. The average total pressure was calculated from the integrated average pressure of each rake. The plane in which the ends of the total tubes were located is shown in figure 5. Orifice spacing is given in the table as distance (y/r) from the model centerline where r is the model inside radius.

A comparison of flow profiles at the rake measured in the static test facility and the wind tunnel is shown in figure 9. Although data are shown for the maximum-reheat plug only, the agreement between profiles in the static and wind tunnel tests as well as the flow symmetry and low distortion levels is typical of all configurations tested.

RESULTS AND DISCUSSION

Nozzle Performance

In order to facilitate comparison of nozzle performance, a flight schedule was assumed that is typical of multimission aircraft. The variation of nozzle pressure ratio with Mach number for this schedule is presented in figure 10. Maximum reheat was as-

sumed for takeoff, which will be considered quiescent conditions. No reheat was assumed for subsonic acceleration. Reheat was assumed for supersonic acceleration, and the nozzle pressure ratio will be the same for both maximum and part reheat.

Two-position shroud nozzle. -

Shroud retracted: The performance of the two-position shroud nozzle with the shroud retracted is presented in figure 11. Experimental data for the cruise plug, part-reheat plug, and maximum-reheat plug are presented in figures 11(a) to (c), respectively. The ratio of measured nozzle thrust-to-ideal thrust (nozzle efficiency) is plotted as a function of nozzle pressure ratio, and ideal thrust was based on the measured weight flow and the nozzle pressure ratio. Both static and wind tunnel results are included. Flags are used to differentiate data obtained for decreasing pressure ratio from that obtained for increasing pressure ratio.

A limited amount of quiescent data was also obtained in the wind tunnel. The ambient pressure was atmospheric for these data; thus, flow system limitations resulted in nozzle pressure ratios generally less than 5. The data obtained in the wind tunnel agreed well with that obtained in the static test facility except for the maximum-reheat plug-retracted shroud (fig. 11(c)). Data repeatability was good, as seen by the agrement between data for increasing and decreasing nozzle pressure ratio.

Maximum values of quiescent nozzle efficiency were 0.977, 0.987, and 0.986 for the cruise, part-reheat, and maximum-reheat plugs, respectively. These maximum values occurred near a pressure ratio corresponding to a Prandtl-Meyer turning angle equal to the throat inclination angle. These pressure ratios are listed in table I (P_7/p_0) and are indicated as tick marks on the abscissa. At higher pressure ratios, the performance was generally characteristic of an underexpanded nozzle.

External flow effects were greater at supersonic Mach numbers than at subsonic Mach numbers. The magnitude of the external flow effect at a given Mach number varied with nozzle pressure ratio.

Shroud extended: The underexpansion losses observed for the retracted shroud nozzles (fig. 11) indicate that a retracted shroud geometry is acceptable for only a limited range of flight conditions. Obviously, internal expansion must be provided such that the performance is optimized at all nozzle pressure ratios. The translating shroud concept has been examined as reported in references 2 and 3. The two-position shroud is a variation of this concept in that a less-complex, single-shroud extension is used. The performance of the two-position shroud with the shroud extended is presented in figures 12(a) to (c) for the cruise, part-reheat, and maximum-reheat plugs, respectively. Only a limited amount of data were obtained for the cruise plug since aircraft thrust requirements would probably dictate a reheat-plug configuration.

Maximum quiescent performance occurred near the pressure ratio for isentropic flow expansion through the internal area ratio. This pressure ratio is indicated by tick marks

on the abscissa and is listed in table I. Maximum nozzle efficiency was 0.966 for the part-reheat plug and 0.972 for the maximum-reheat plug. Performance decreased sharply below the indicated pressure ratio since the nozzles are overexpanded. At higher pressure ratios, the performance of the maximum-reheat plug decreased sharply compared to that of the part-reheat plug. This phenomenon is characteristic of an area ratio effect on the performance of underexpanded nozzles. Free-stream effects at a given Mach number varied with nozzles pressure ratio, which agrees with observations made for the retracted shroud.

Floating shroud nozzle. - The performance of the floating shroud nozzle is shown in figure 13(a) for the cruise plug, 13(b) for the part-reheat, and 13(c) for the maximum-reheat plug. The quiescent nozzle performance of all plugs tested was maximum and nearly constant between the minimum and maximum pressure ratios indicated by tick marks on the abscissa. These points were determined by the shroud stops, as discussed in the nozzle description. Maximum quiescent efficiency was 0.978, 0.984, and 0.989 for the cruise, part-reheat, and maximum-reheat plugs, respectively. Below the minimum indicated pressure ratio, the nozzles were typically overexpanded. Although the nozzles were underexpanded above the maximum indicated pressure ratio, the decrease in performance was gradual in contrast to that of the two-position shroud.

External flow effects at a given Mach number varied with nozzle pressure ratio as observed for the two-position shroud. However, for the part-reheat plug, the external flow effects tended to generalize at supersonic Mach numbers within the range of nozzle pressure ratios tested.

Only a limited amount of external flow data was obtained for the maximum-reheat plug, due to a failure of the floating shroud hardware. Post-test analysis indicated that the failure resulted from model design considerations rather than an aerodynamic flutter problem.

Comparative nozzle performance for assumed flight schedule. - The performance of the two-position shroud nozzle at the assumed flight conditions is shown in figure 14. Faired nozzle performance curves are repeated from figure 11 for the retracted shroud (solid lines) and figure 12 for the extended shroud (dashed lines). Symbols denote flight operating conditions; that is, Mach number and nozzle pressure ratios from figure 10. In general, the nozzle operating conditions were below the nozzle pressure ratio for peak performance at a given Mach number. In particular, the cruise point (solid symbols in fig. 14(a)) was at Mach 0.85, $P_7/p_0 = 3$; and the nozzle efficiency was 0.932. The maximum nozzle efficiency measured at Mach 0.85 was 0.956 and occurred at $P_7/p_0 = 5.4$. The performance for both part reheat (fig. 14(b)) and maximum reheat (fig. 14(c)) indicates that for best flight performance the shroud should be retracted at Mach numbers less than 1.2. For example, the nozzle efficiency for maximum reheat at Mach 0.85 was 0.967 with the shroud retracted and 0.926 with the shroud extended. At Mach 1.2, the

nozzle efficiencies were nearly equal: 0.933 and 0.922 for the retracted and extended shroud, respectively.

The performance of the floating shroud nozzle at assumed flight conditions is shown in figure 15. Faired performance curves are repeated from figure 13, and symbols denote the flight operating conditions. As noted for the two-position shroud configurations, nozzle efficiency at the flight operating conditions was less than the maximum efficiency measured at a given Mach number.

A comparison of nozzle performance for the two-position and floating shroud is shown in figure 16. Part reheat was assumed for transonic acceleration. Nozzle efficiency is plotted as a function of Mach number and was obtained from the flight operating points shown in figures 14 and 15. (Takeoff efficiency for the floating shroud was obtained from fig. 13(c).) Flight Mach numbers used are indicated by tick marks. Solid and dashed lines distinguish the two-position and floating shrouds, respectively. The performance advantage of a retracted shroud at Mach numbers less than 1.2 can clearly be seen. The following conclusions are indicated from the performance comparison: At takeoff and subsonic cruise, both configurations are nearly comparable in performance. For example, at takeoff (open symbols) the nozzle efficiency for the two-position shroud was 0.964, whereas that of the floating shroud was 0.968. At the cruise point (solid symbols), the nozzle efficiencies were 0.932 and 0.930 for the two-position and floating shroud, respectively. However, the two-position shroud had better performance for subsonic acceleration, whereas the floating shroud had better performance at supersonic Mach numbers. The nozzle efficiencies of the two-position and floating shrouds, respectively, were 0.959 and 0.943 at Mach 0.56, and 0.928 and 0.948 at Mach 1.97.

The performance loss due to free-stream effects is shown in figure 17 and assumes part reheat for transonic acceleration. The loss is defined as the difference between quiescent nozzle efficiency and nozzle efficiency at a given Mach number. It was calculated (in percent of ideal thrust) for the assumed flight schedule. Maximum free-stream effects occurred at Mach 1.2. Performance loss was as high as 5.1 percent of ideal thrust for the two-position shroud nozzle and 5.8 percent for the floating shroud nozzle. Both shroud configurations had nearly the same loss at the subsonic cruise point (solid symbols): 4.1 percent for the two-position shroud and 4.2 percent for the floating shroud.

Plug Pressure Distributions

Plug pressure distributions for a propulsive jet exhausting into still air are determined by the normal jet parameters that affect the jet structure (i.e., nozzle pressure ratio, exit Mach number, specific heat ratio). When the jet exhausts into an external flow, parameters such as free-stream Mach number, local ambient pressure, and the

geometry of the nozzle installation also affect the plug pressure distributions. This is the result of jet and free-stream interaction which modifies the flow structure. Reference 4 presents results of an experimental and theoretical study concerning the structure of axisymmetric free jets and the effects of a supersonic external stream. Concepts of jet structure presented therein may also apply to the flow field of plug nozzles. However, the concepts must be modified to account for the fact that the plug nozzle has an annular discharge, and the inner flow boundary is limited by the plug, while the outer boundary is formed by the free-jet expansion to ambient conditions.

Schematics of the flow field for a conical plug nozzle are presented in figure 18 for both quiescent and external flow. The general case of a double-angle plug was assumed, thus simulating a collapsible plug nozzle (part-reheat configuration). The retracted shroud geometry was assumed in figure 18, providing an example of a sonic discharge. The assumption was made that the nozzle pressure ratio was greater than 2.0 and that a supersonic external Mach number existed.

Retracted shroud. - In the case of a retracted shroud nozzle exhausting into still air (fig. 18(a)), the flow expands about the shroud from Mach 1.0 to a supersonic Mach number determined by the nozzle pressure ratio. Typical expansion waves associated with this turning are shown as dotted lines. The expansion waves are reflected from the plug surface as expansion waves because flow at the plug is bounded by the diverging plug surface which does not cancel the expansion fan. Therefore, an overexpanded region exists immediately downstream of the exit wherein plug pressures are less than ambient pressures (region 1). This overexpansion phenomenon has been observed in other plug nozzle studies as reported, for example, in reference 5. Expansion waves reflected from the plug are, in turn, reflected from the flow boundary as compression waves of equal strength (solid lines), resulting from the fact that the diverging jet turns back to the axial direction so that a constant pressure is maintained along the flow boundary. These compression waves are then reflected from the plug as compression waves, producing a region of increasing plug pressures (region 2). The reflected compression waves coalesce to a region within the jet, where conditions at the discharge are repeated; and the entire process of expansion and recompression is repeated. However, the process is slightly modified by expansion about the hinge point and the change in surface angle. Theoretically, the periodic nature of the flow field should continue ad infinitum; but in the real gas, shock losses and friction effects result in a gradual decrease in jet energy. Thus, the plug pressure distributions should show a cyclic expansion and compression with decreasing maxima and minima tending to a constant value equal to ambient pressure.

The characteristics of the nozzle flow field, therefore the plug pressures, might be expected to change due to the effect of an external flow. Clearly, installation effects that significantly alter the local ambient flow conditions may result in an altered nozzle flow field. Furthermore, the jet flow is altered due to the interaction of the jet plume and the

external flow. In the case of a subsonic external flow, this interaction consists of viscous mixing along the jet boundary and does not significantly alter the constant pressure flow boundary. Therefore, the jet structure should not change from the quiescent case. Hence, the plug pressure distributions will not be significantly affected by a subsonic external flow.

Consider next the case of a supersonic external stream. The expansion fan, associated with flow expansion to ambient pressures, produces a region of overexpansion on the plug (region 1 of fig. 18(b)) as discussed for the case of quiescent flow. However, the external flow imposes a static pressure gradient on the jet boundary because of the pressure rise across the trailing shock generated in the supersonic stream. Thus, the local ambient pressure may be altered and, hence, will influence the initial overexpansion on the plug surface. In addition, the jet boundary is no longer constrained to be at constant static pressure along its length. Hence, reflected waves from the plug surface are not required to reflect from the jet boundary as equal-strength, opposite waves. Furthermore, the impinging wave may be transmitted into the external flow and only partially reflected back to the plug surface. The jet structure will have the same periodic character as that for still air; however, the strength of the first recompression and subsequent overexpansion regions should be reduced, and the regions should be spread over larger plug areas. Reference 4 points out that, in effect, the jet flow resembles that of a jet exhausting into still air, but at a lower nozzle pressure ratio.

Plug pressure distributions for the two-position shroud nozzle with the shroud retracted are presented in figure 19. Cruise plug pressure distributions are shown in figures 19(a) to (e), part-reheat in figures 19(f) and (g), and maximum-reheat in figures 19(h) and (i). Plug local-to-ambient pressure ratio is plotted as a function of the nondimensional distance from the plug throat station (x/l). Quiescent data (flagged) is compared to data with external flow at nozzle pressure ratios approximating the assumed nozzle pressure ratio schedule shown in figure 10. Pressure distributions for all plugs with and without external flow show overexpansion just downstream of the exit, as explained in the discussion of the flow field (region 1 of fig. 18). As expected, the expansion region increases with nozzle pressure ratio. For example, the cruise plug expansion region extended to an x/l of 0.06 for a low pressure ratio (fig. 19(a)) and an x/l of 0.17 for a high pressure ratio (fig. 19(e)). Since the overexpansion occurs in a region of large projected areas, it may represent a significant performance loss. Conceivably an isentropic contour in this region could improve the subsonic performance of these configurations.

The recompression (region 2 of fig. 18) associated with initial overexpansion can be observed for all configurations. At subsonic Mach numbers (figs. 19(a) to (c) and (f) for the cruise and part-reheat plugs, respectively), the recompression and subsequent cyclic variation in plug pressures agrees well with the quiescent data. This observation supports the contention that the flow field of a jet exhausting into a subsonic stream exhibits

the same cyclic pattern of expansion and compression as a jet exhausting into still air. The exception noted for the maximum-reheat plug at Mach number 0.85 (fig. 19(h)) may result from the higher nozzle pressure ratio of the external flow data ($P_7/p_0 = 4.1$, compared to $P_7/p_0 = 3.41$). The decay of maximum and minimum values of pressure ratio is indicative of energy dissipation within the jet.

At supersonic Mach numbers (figs. 19(d) and (e), (g) and (i) for the cruise, part-reheat, and maximum-reheat plugs, respectively), the recompression region and subsequent pressure distribution differs from the quiescent data. This observation exemplifies the reduced strength of the recompression due to the jet-free stream interaction. The noncyclic nature of the pressure distributions, particularly for the cruise plug indicates that the recompression shocks may not be reflected from the jet mixing boundary at these pressure ratios, resulting in a damped flow field.

The performance loss represented by the difference in plug pressure distributions with and without external flow was calculated for the cruise plug at $M_0 = 1.2$, $P_7/p_0 = 5.07$ and 7.05 (see figs. 19(d) and (e)). These conditions are not on the assumed flight schedule but were chosen as illustrative examples of the performance loss. This loss was defined as the difference in integrated pressure force between quiescent data and external flow data. Estimates of boattail drag including jet effects at these conditions were calculated using the method of reference 6. At a nozzle pressure ratio of 5.7, the nozzle efficiency presented in figure 11(a) indicates a total difference of 10.2 percent of ideal thrust between quiescent data and data at Mach 1.2. The calculated boattail drag was approximately 3.5 percent of ideal thrust and the loss due to plug pressure force was 5 percent, thus accounting for nearly all the loss within the limitations of the calculation. At a pressure ratio of 7.05, the total loss was 5 percent. The boattail drag was 2 percent, and the plug pressure force loss was 3 percent and accounted for the total loss.

Extended and floating shroud. - A schematic diagram of the nozzle flow field with an extended shroud is shown in figure 20. An extended shroud as well as a floating shroud imposes a pressure gradient on the flow between the throat and shroud exit unlike the constant pressure boundary for the retracted shroud. The plug pressures in this internal expansion will be typical of a convergent-divergent nozzle (region 1 of fig. 20). Ideally, the shroud extension or floating shroud position should be such that the shroud exit and ambient pressure are equal; and pressures downstream of the shroud exit would remain at ambient pressure. Conversely, if the internal flow is overexpanded or underexpanded, recompression or continued expansion will occur downstream of the shroud exit. The flow schematic for the extended shroud nozzle with and without external flow (shown in figs. 20(a) and (b), respectively) assumes an overexpanded internal flow. This condition exists at nozzle pressure ratios less than 12, 7, and 4.7 for the maximum-reheat, part-reheat, and cruise plugs, respectively. Thus, the nozzle flow compresses at the shroud

exit resulting in a recompression zone (region 2) on the plug. Included in the recompression region are compression waves from the internal shroud surface since the plug is diverging whereas the shroud is cylindrical. For the quiescent case, the inward compression waves in region 2 reflect from the plug surface as outward compression waves that coalesce; and the process of expansion and recompression is periodic as discussed for the retracted shroud. In the case of supersonic external flow, the inward compression waves in region 2 are reflected from the plug as compressions and coalesce to begin the second cycle of expansion and compression. Since the jet plume is converging at the exit, the jet-stream interaction occurs during the second cycle. Thus the plug pressures in the initial recompression (region 2) should agree with quiescent data. This would not be true of an underexpanded internal flow. The initiation of a second cycle and, for that matter, any subsequent cycles again depends on the nature of the wave reflection and transmission into the external flow at the jet mixing boundary. Therefore, for the extended shroud and supersonic external flow, the plug pressure distributions might differ from those for still air at a further distance along the plug than observed for the retracted shroud.

Plug pressure distributions for the two-position shroud nozzle with the shroud extended are presented in figure 21. Part-reheat plug pressure distributions are shown in figures 21(a) to (d), and maximum-reheat in figures 21(e) to (h). For both plugs, the internal flow was overexpanded; but the overexpansion decreased as the nozzle pressure ratio increased toward the design point of the internal expansion. Recompression occurred downstream of the shroud exit even for a fully-expanded or underexpanded internal flow. For example, see figures 21(d), (g), and (h). This phenomenon is indicative of the internal shocks generated from the shroud as explained in the discussion of figure 20. Modification of the flow field due to expansion about the hinge point and the change in surface angle can clearly be seen in the quiescent data for the part-reheat plug in figures 21(c) and (d), and for the maximum-reheat plug in figures 21(e) to (h). In general, the external flow distributions differed from the quiescent data after the expansion of the second cycle, which indicates that the jet free-stream interaction and subsequent damping of jet recompression occurs further downstream for the extended shroud geometry. The notable exception was the part-reheat plug at Mach 1.2 (fig. 21(a)) where the initial recompression was damped.

Plug pressure distributions for the floating shroud nozzle are shown in figures 22(a) to (h). Data for the cruise plug (figs. 22(a) and (b)) show that the floating shroud tended to expand the flow to ambient pressure at the shroud exit, although a slight overexpansion occurred. Also, pressures for the part-reheat plug (figs. 22(c) to (g)) indicated that the internal flow was only moderately overexpanded. However, the initial expansion continued beyond the shroud exit and resulted in increased overexpansion. As observed for the retracted shroud, plug pressures for subsonic Mach numbers agreed with quiescent

data. At supersonic Mach numbers, plug pressures diverged from quiescent data but at high values of x/l, thus agreeing with observations for the extended shroud concerning the delayed jet-stream interaction.

SUMMARY OF RESULTS

An experimental study was made concerning the effects of two types of shroud geometry on the performance of a collapsible plug nozzle. Shroud geometries considered were a cylindrical, two-position shroud and a variable angle floating shroud. Quiescent performance was obtained at nozzle pressure ratios from 2 to 15, and external flow effects were obtained at Mach numbers from 0.56 to 1.97. For an assumed schedule of pressure ratio and Mach numbers from 0.56 to 1.97. For an assumed schedule of pressure ratio and Mach number, the following results were obtained:
nearly comparable at takeoff and subsonic cruise. For example, at takeoff, the nozzle efficiency for the two-position shroud was 0.964, whereas that of the floating shroud was 0.968. At the cruise point, Mach 0.85, the nozzle efficiencies were 0.932 and 0.930 for the two-position shroud and floating shroud, respectively. However, the two-position shroud had better performance for subsonic acceleration, whereas the floating shroud had better performance at supersonic Mach numbers. The nozzle efficiencies of the two-position and floating shroud, respectively, were 0.959 and 0.943 at Mach 0.56, and 0.928 and 0.948 at Mach 1.97.

2. The two-position shroud should be retracted at Mach numbers less than 1.2 for optimum nozzle performance.

3. External flow effects were greatest at Mach 1.2 for both shroud geomtries. The maximum performance loss for the two-position and floating shrouds, respectively, was 5.1 percent and 5.8 percent of ideal thrust.

4. A supersonic external stream can modify the expansion and compression regions in the plug nozzle exhaust thus changing the plug pressure level and distribution from that measured statically. The change in plug pressure force may represent a significant loss in performance.

Lewis Research Center,
National Aeronautics and Space Administration,
Cleveland, Ohio, May 21, 1968,
126-15-02-10-22.

REFERENCES

1. Smith, K. G.: Methods and Charts for Estimating Skin Friction Drag in Wind Tunnel Tests with Zero Heat Transfer. Rep. ARC-CP-824, Aeronautical Research Council, Great Britain, 1965.

2. Bresnahan, Donald L.; Johns, Albert L.: Cold Flow Investigation of a Low Angle Turbojet Plug Nozzle with Fixed Throat and Translating Shroud at Mach Numbers from 0 to 2.0. NASA TM X-1619, 1968.

3. Herbert, M. V.; Golesworthy, G. T.; and Herd, R. J.: The Performance of a Centre Body Propelling Nozzle with a Parallel Shroud in External Flow, Part II. Rep. ARC-CP-894, Aeronautical Research Council, Great Britain, 1966.

4. Love, Eugene S.; Grigsby, Carl E.; Lee, Louise P.; and Woodling, Mildred J.: Experimental and Theoretical Studies of Axisymmetric Free Jets. NASA TR R-6, 1959.

5. Schmeer, James W.; Kirkham, Frank S.; and Salters, Leland B., Jr.: Performance Characteristics of a 10^{o} Conical Plug Nozzle at Mach Numbers up to 1.29. NASA TM X-913, 1964.

6. Benson, J. L.; Miller, L. D.; and Horie, G.: Theoretical Study of Engine Exhaust Nozzle Airframe Integration. Rep. LR-20678, Lockheed-California Co. (AEDC-TR-67-214, DDC No. AD-822074), Oct. 1967.

TABLE I. - NOZZLE GEOMETRY DETAILS[a]

Nozzle geometry	Nozzle throat area, A*		Annular area at nozzle exit, A_9		Area ratio, A_9/A^*		Nozzle pressure ratio, P_7/p_0		Nozzle discharge coefficient, C_{D8} (static test)	Projected boattail area, $A_{Boattail}$		Boattail angle, β, deg
	$in.^2$	cm^2	$in.^2$	cm^2						$in.^2$	cm^2	
Two-position shroud, retracted:												
Maximum reheat-plug	31.80	205	31.80	205	1.0		2.37		0.977	[b]2.67	[b]17.20	[b]8
Part-reheat plug	23.70	153	23.70	153	1.0		2.85		.988	[c]2.04	[c]13.20	[c]8
No-reheat plug	15.59	101	15.59	101	1.0		3.35		.990	[d]4.71	[d]30.40	
Two-position shroud, extended:												
Maximum-reheat plug	31.80	205	41.17	266	1.31		4.73		0.977	[d]2.04	[d]13.20	8
Part-reheat plug	23.70	153	36.95	248	1.60		7.06		.988			
No-reheat plug	15.59	101	33.20	214	2.13		11.95		.990			
			Minimum		Maximum		Minimum	Maximum	Minimum	Maximum		
			$in.^2$	cm^2	$in.^2$	cm^2						
Floating shroud:												
Maximum-reheat plug	31.80	205	33.40	216	45.98	297	1.05	1.45	2.53	5.79	0.983	
Part-reheat plug	23.70	153	30.10	194	42.71	276	1.27	1.80	4.40	8.82	.996	
No-reheat plug	15.59	101	16.83	109	39.91	258	1.08	2.56	2.86	16.26	.999	

Floating shroud:	Minimum $in.^2$	Minimum cm^2	Maximum $in.^2$	Maximum cm^2	Minimum	Maximum
Maximum-reheat plug	3.06	19.8	9.53	61.5	4.46	-3.36
Part-reheat plug	3.06	19.8	9.53	61.5	4.46	-3.36
No-reheat plug	13.56	87.5	9.53	61.5	11.00	-3.36

[a]See figs. 5 and 6.
[b]Internal.
[c]External.
[d]Total.

TABLE II. - PLUG STATIC ORIFICE DISTRIBUTION[a]

Orifice	Maximum reheat			Part reheat			Cruise		
	Axial distance from throat station, x		Distance from throat station, x/l	Axial distance from throat station, x		Distance from throat station, x/l	Axial distance from throat station, x		Distance from throat station, x/l
	in.	cm		in.	cm		in.	cm	
1	0.10	0.254	0.0054	0.09	2.28	0.0049	0.10	0.254	0.0055
2	.66	1.67	.0358	.61	1.55	.0332	.55	1.40	.030
3	1.22	3.10	.0663	1.15	2.92	.0627	1.01	2.56	.0552
4	1.78	4.52	.0966	1.69	4.30	.0921	1.48	3.78	.0808
5	2.36	6.00	.128	2.24	5.70	.122	1.97	5.00	.1075
6	2.93	7.44	.159	2.82	7.16	.154	2.57	6.53	.1403
7	3.53	8.96	.192	3.41	8.65	.186	3.09	7.85	.1687
8	4.13	10.48	.224	4.01	10.20	.219	3.63	9.22	.198
9	4.72	11.98	.256	4.65	11.80	.253	4.18	10.60	.228
10	5.34	13.54	.290	5.28	13.40	.287	4.75	12.10	.259
11	5.97	15.15	.324	5.95	15.10	.324	5.35	13.60	.292
12	6.61	16.77	.359	6.65	16.90	.362	5.98	15.20	.327
13	7.32	18.60	.398	7.27	18.50	.396	6.64	16.90	.362
14	7.52	19.10	.408	7.47	19.00	.407	7.42	18.80	.405
15	8.68	21.80	.471	8.63	21.90	.470	8.58	21.80	.468
16	10.05	25.50	.546	10.0	25.40	.545	9.95	25.20	.543
17	11.63	29.60	.632	11.58	29.40	.631	11.53	29.30	.630
18	13.71	34.80	.745	13.66	34.70	.744	13.61	34.60	.743
19	16.19	41.10	.879	16.14	41.00	.880	16.09	40.80	.878

[a]See fig. 7.

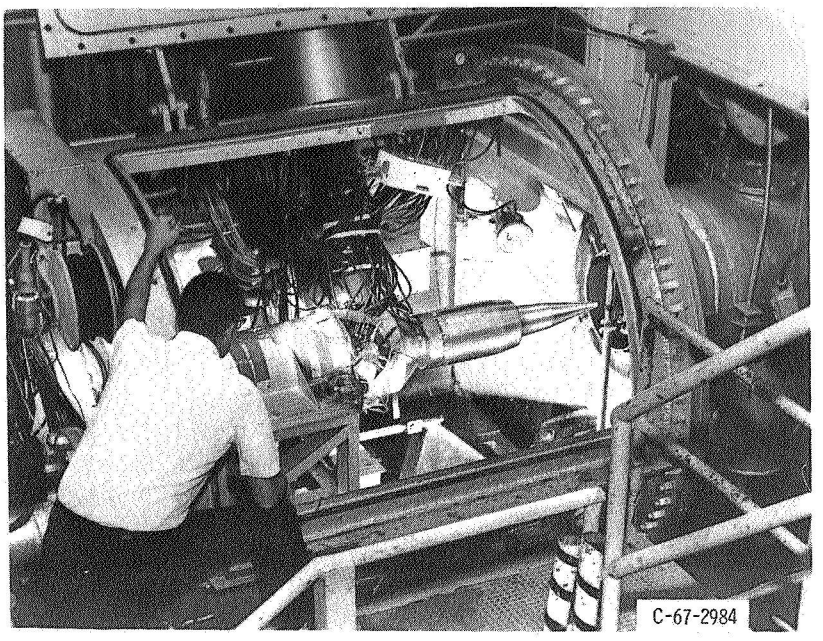

Figure 1. - Model installation in quiescent test facility.

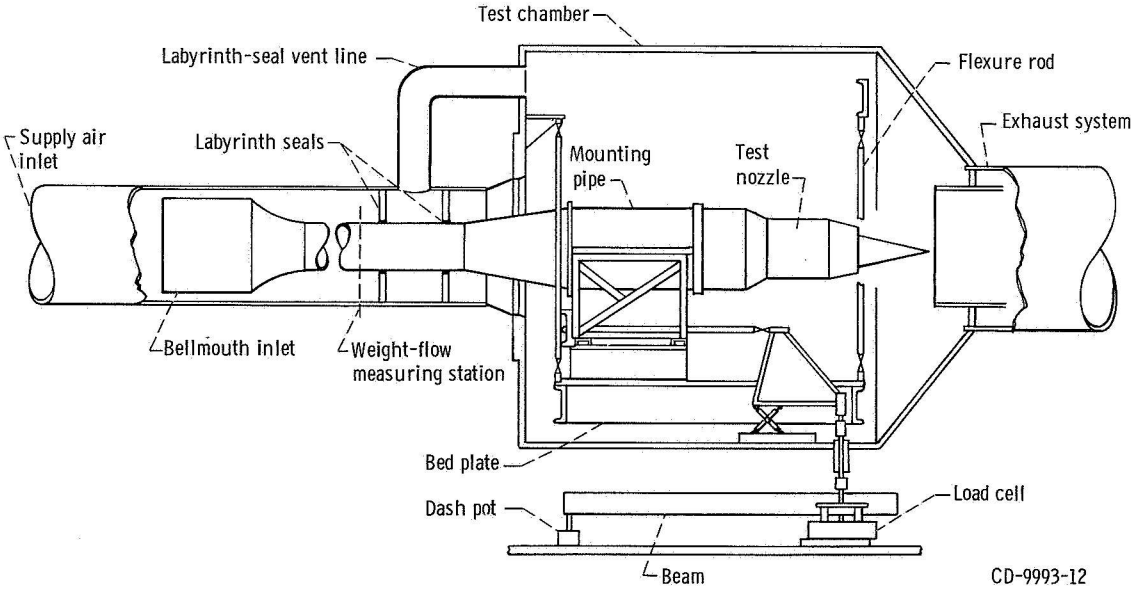

Figure 2. - Schematic of model installation in quiescent test facility.

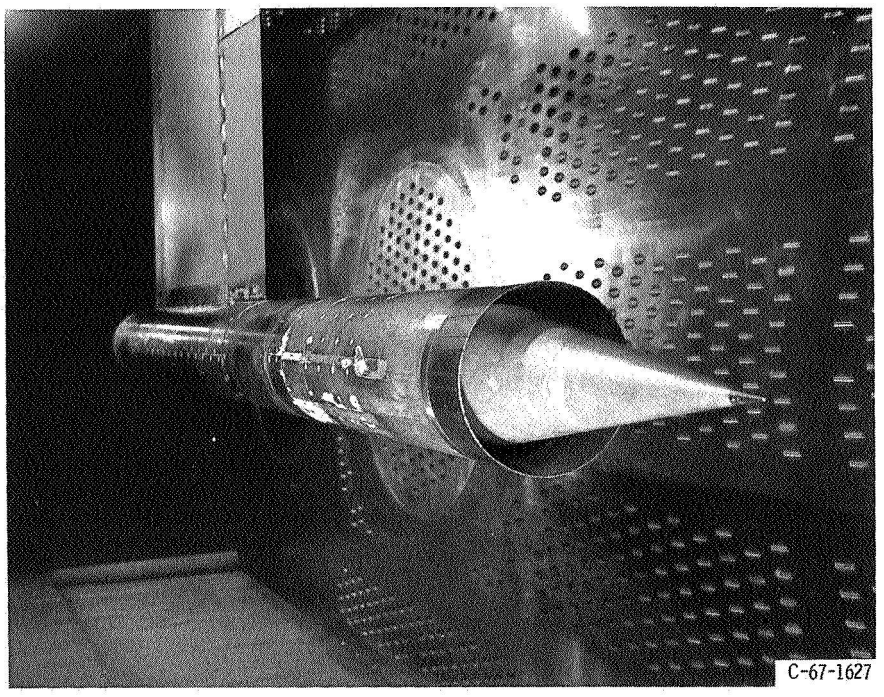

Figure 3. - Model installation in wind tunnel.

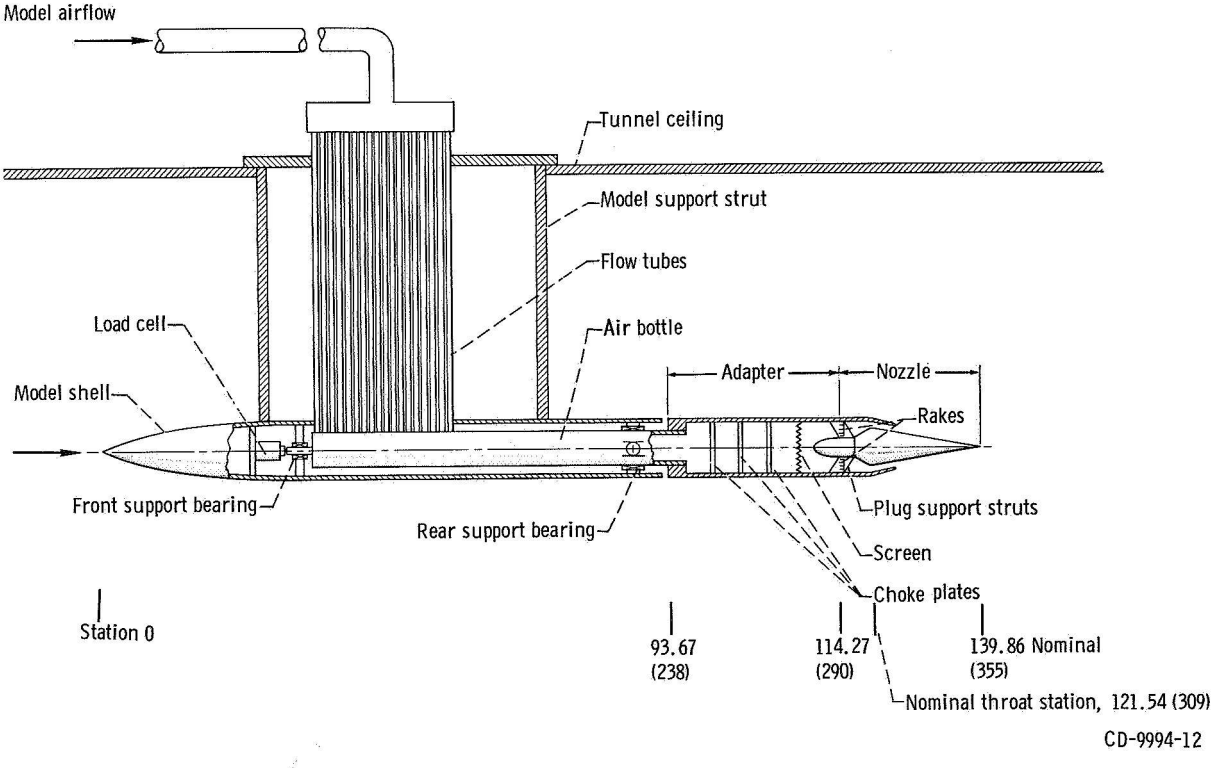

Figure 4. - Wind tunnel model internal geometry and thrust measuring system. (Dimensions in inches (cm).)

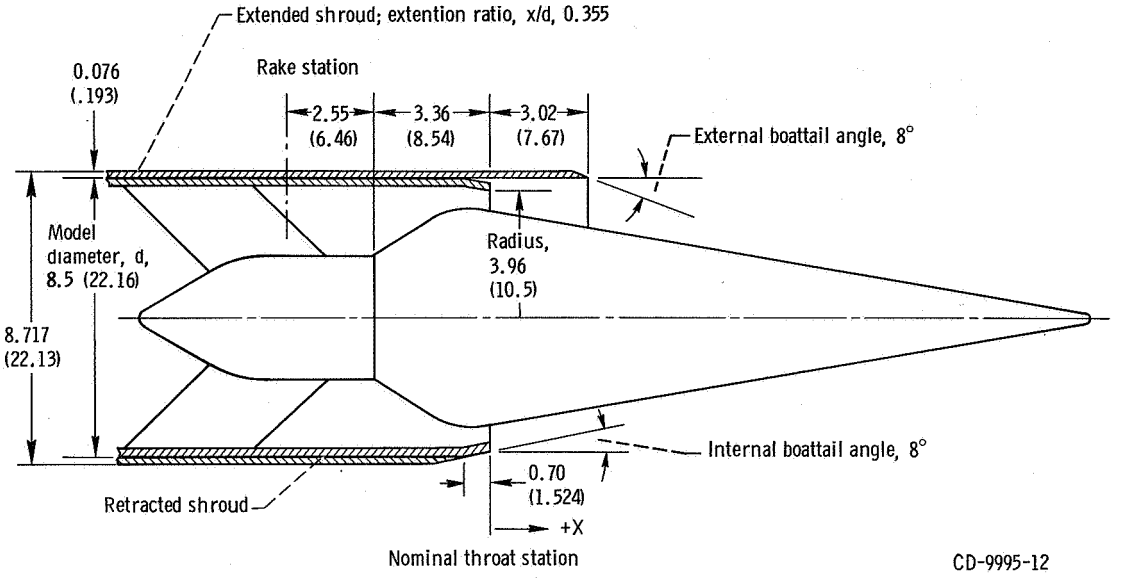

(a) Two-position shroud.

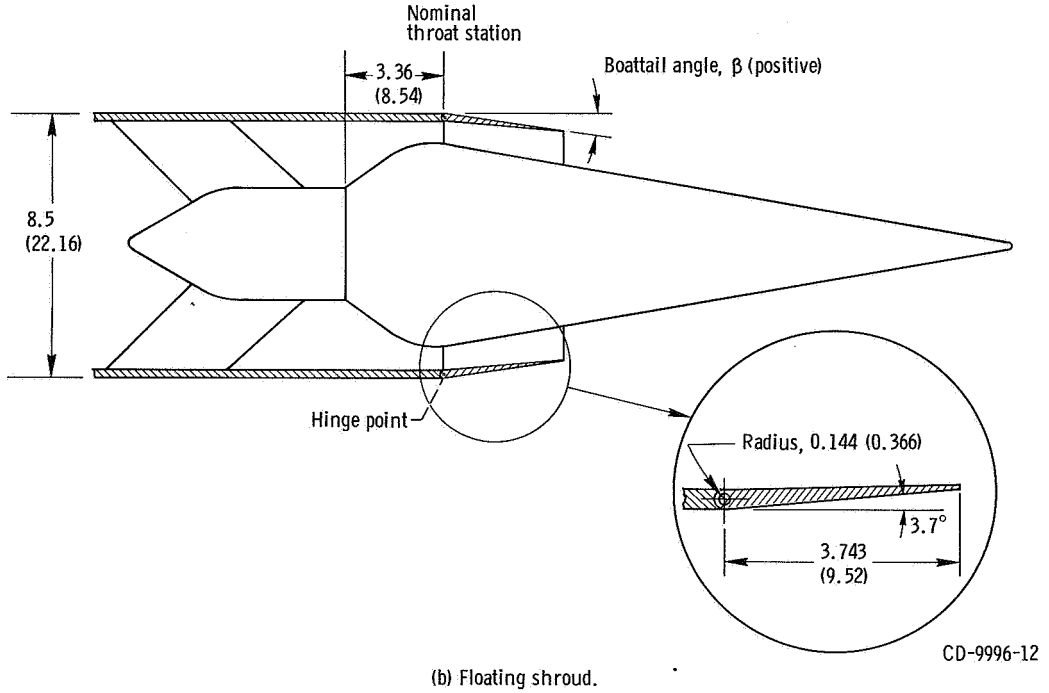

(b) Floating shroud.

Figure 5. - Details of nozzle shroud. (Dimensions in inches (cm).)

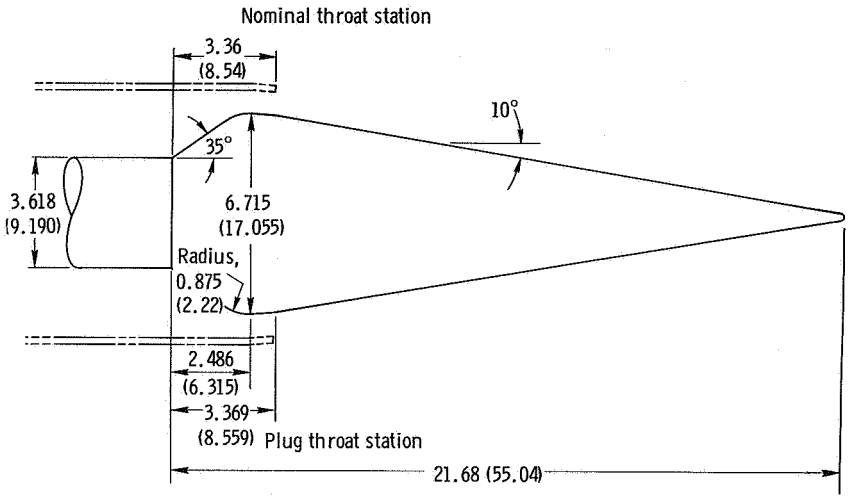

(a) Cruise plug.

CD-9997

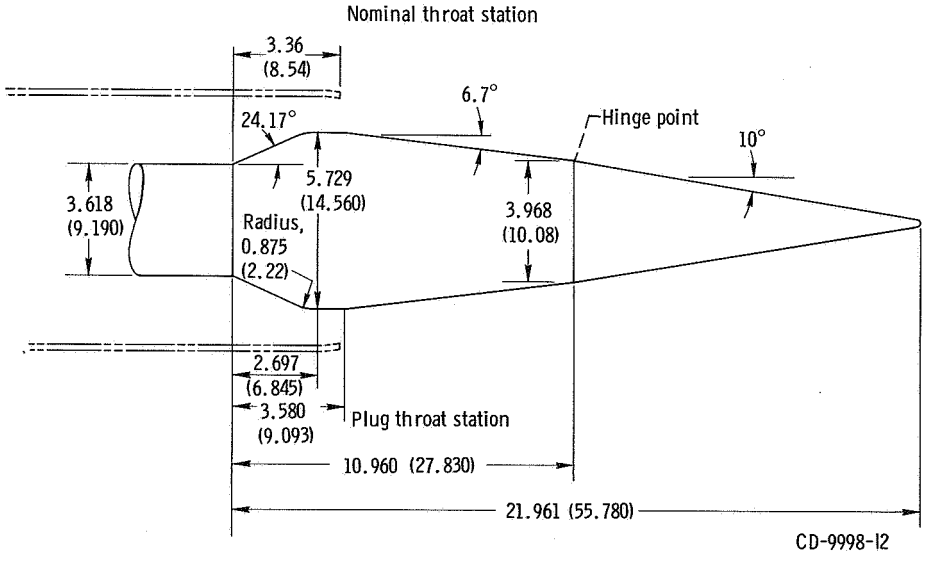

CD-9998-12

(b) Part-reheat.

Figure 6. - Plug details. (Dimensions in inches (cm).)

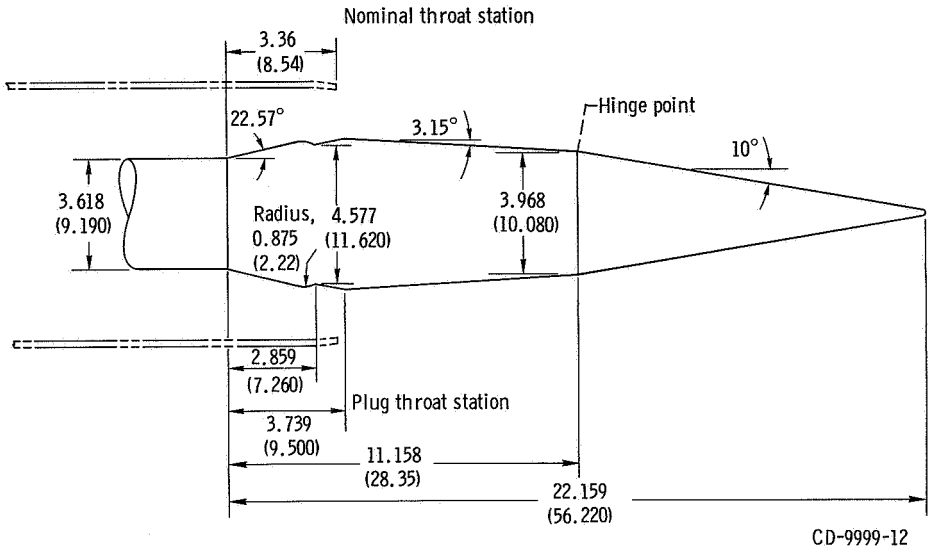

(c) Maximum-reheat.

Figure 6. - Concluded.

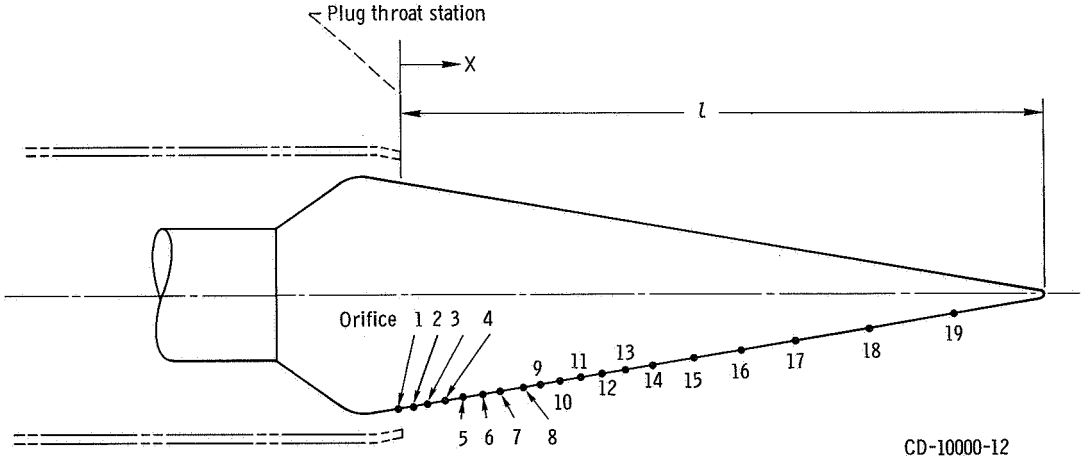

Figure 7. - Typical plug static-pressure instrumentation.

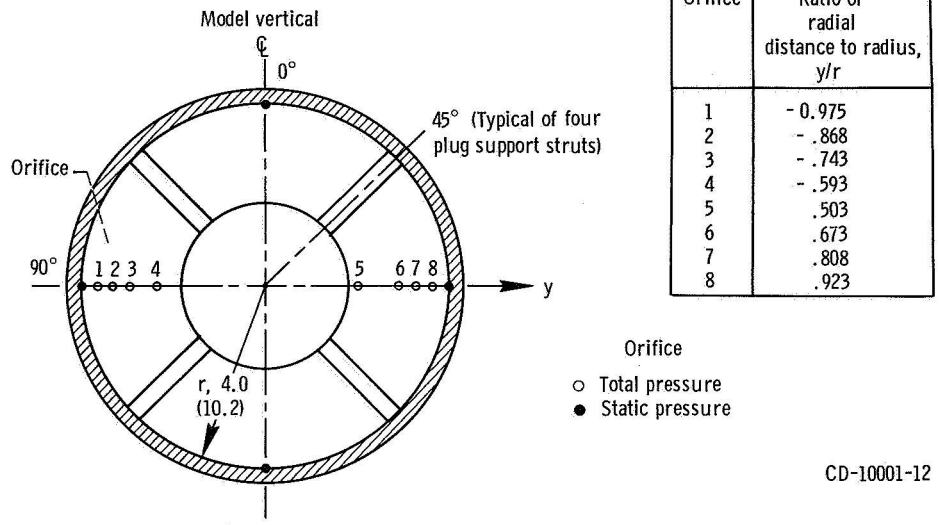

Orifice	Ratio of radial distance to radius, y/r
1	-0.975
2	-.868
3	-.743
4	-.593
5	.503
6	.673
7	.808
8	.923

Figure 8. - Details of rake instrumentation. Model section at rake station, view looking upstream. (Dimensions in inches (cm).)

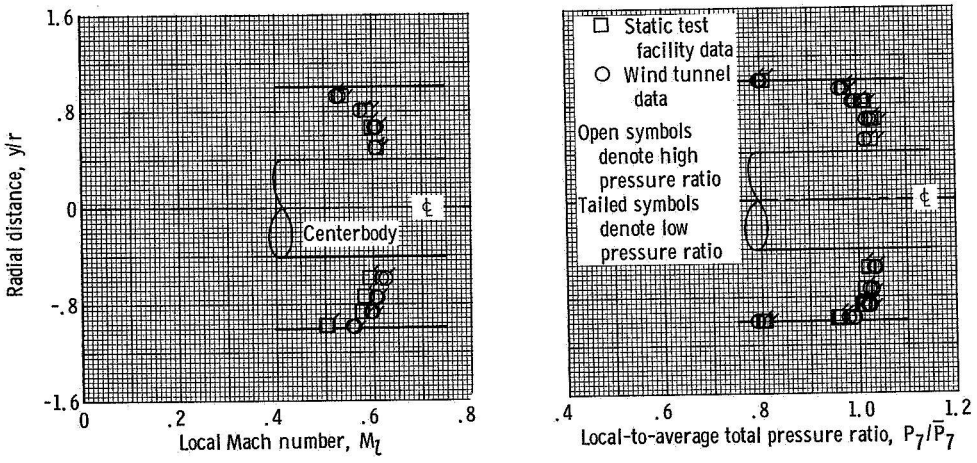

Figure 9. - Flow profiles at rake station, maximum reheat plug.

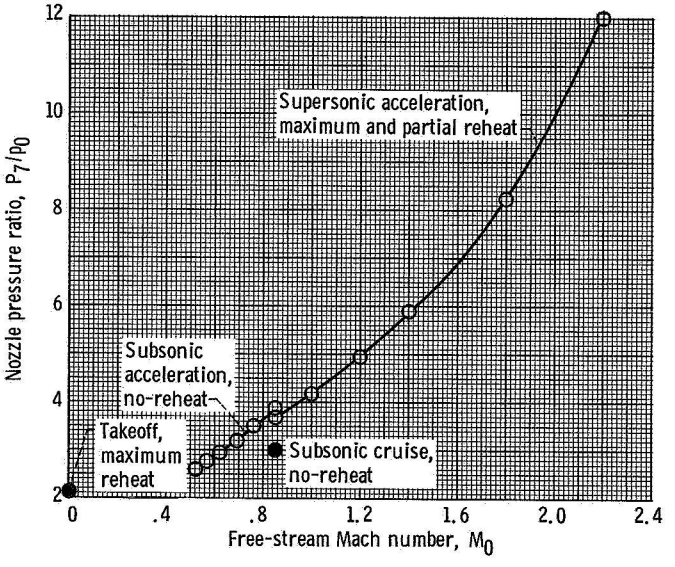

Figure 10. - Assumed schedule of nozzle pressure ratio.

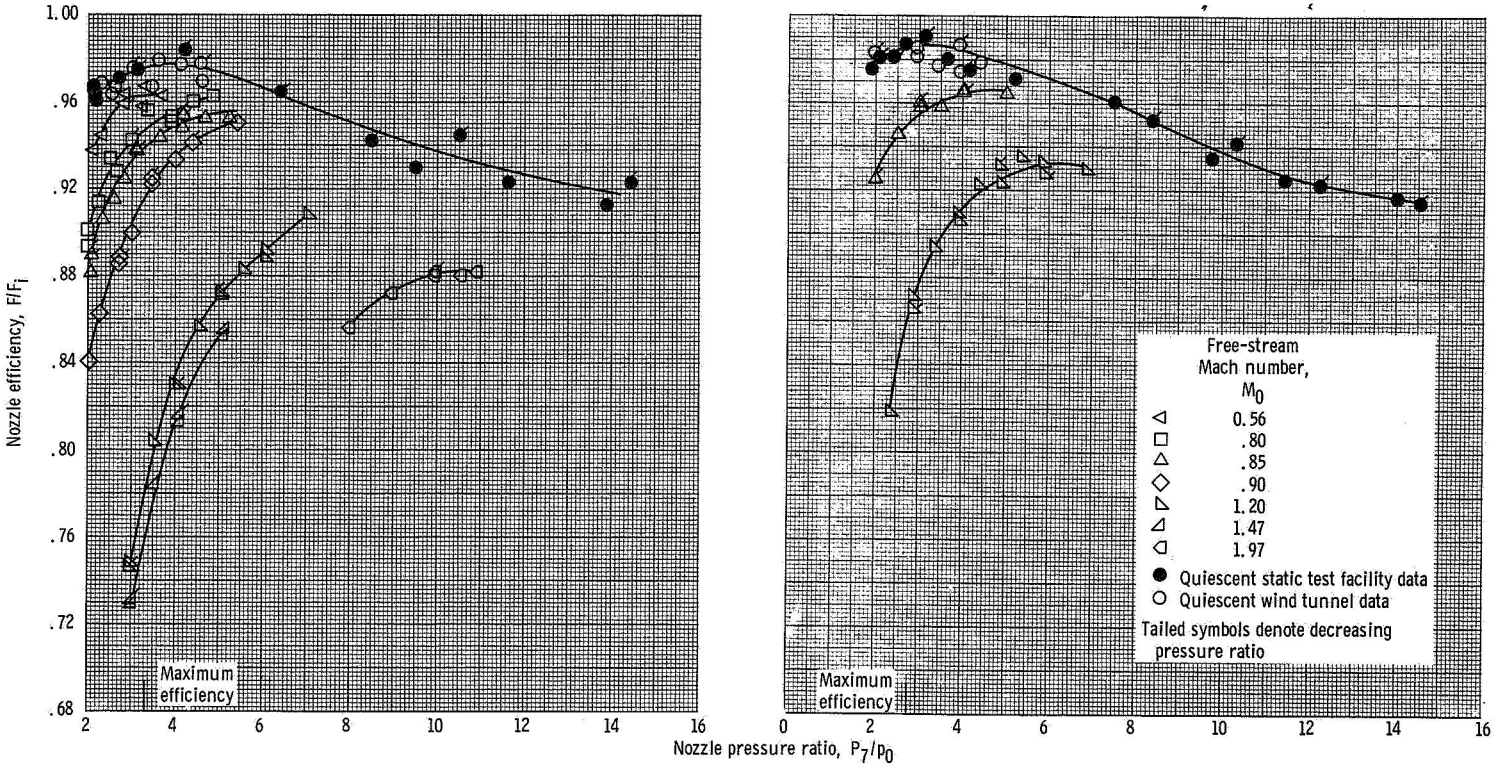

(a) Cruise plug.

(b) Part-reheat plug.

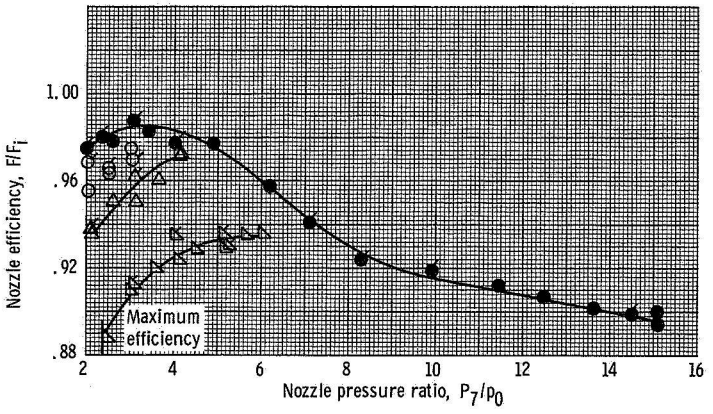

(c) Maximum-reheat plug.

Figure 11. - Performance of two-position shroud nozzle, shroud retracted.

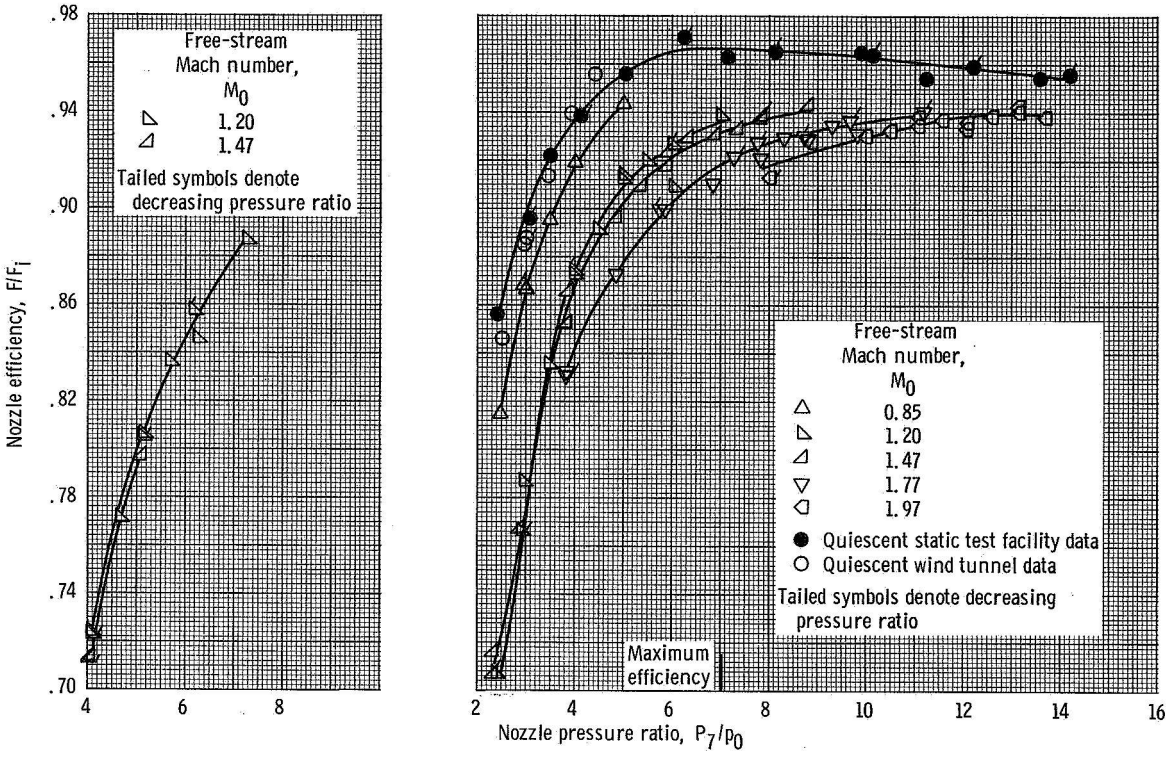

(a) Cruise plug.

(b) Part-reheat plug.

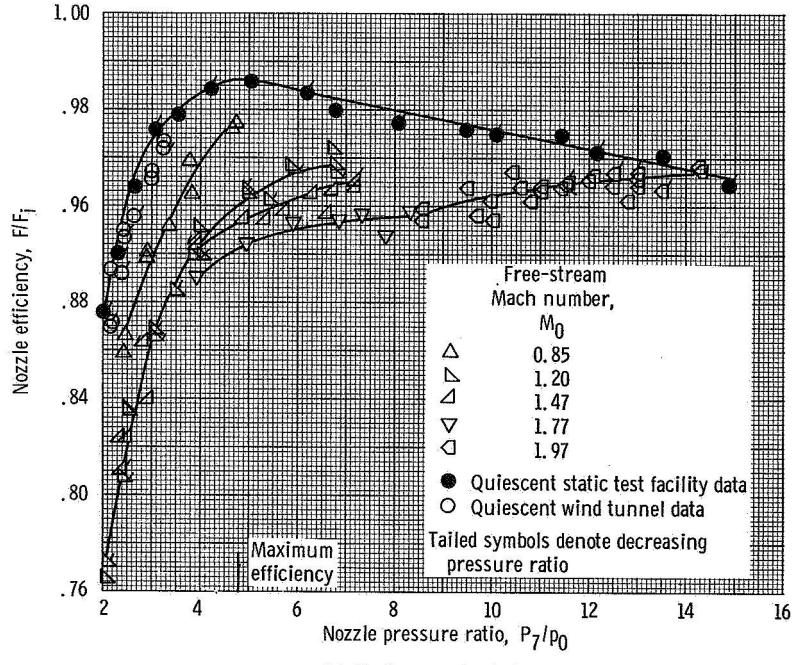

(c) Maximum-reheat plug.

Figure 12. - Performance of two-position shroud nozzle, shroud extended.

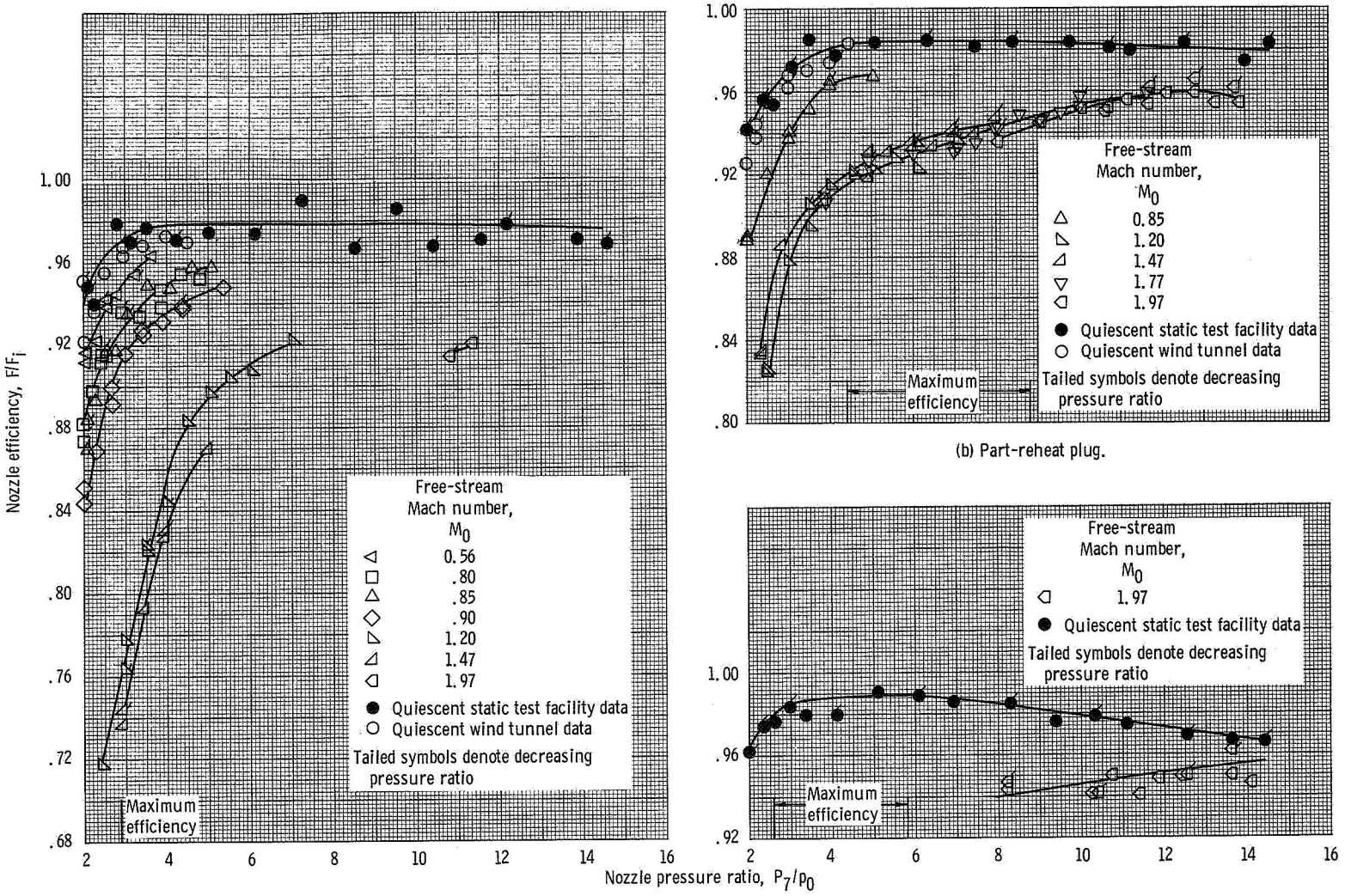

(a) Cruise plug.

(b) Part-reheat plug.

(c) Maximum-reheat plug.

Figure 13. - Performance of floating shroud nozzle.

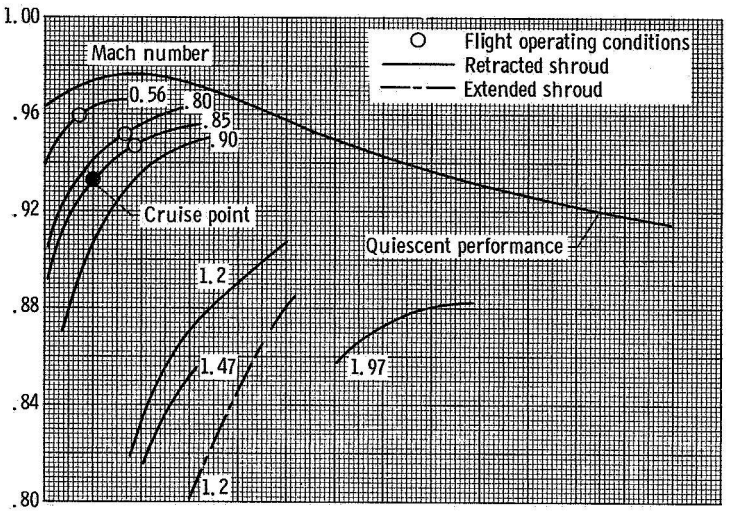

(a) No-reheat.

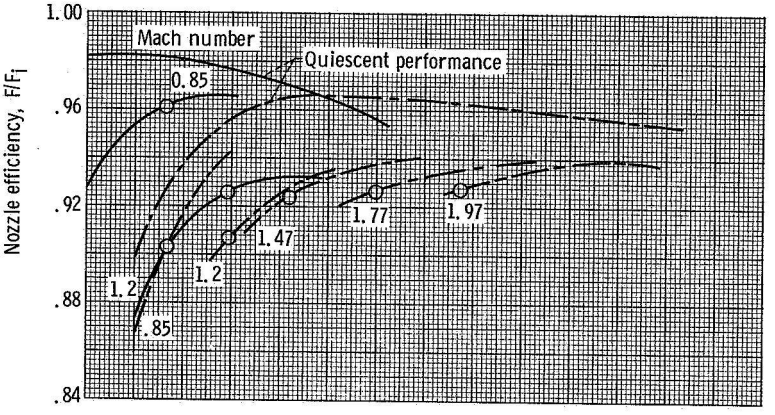

(b) Part-reheat.

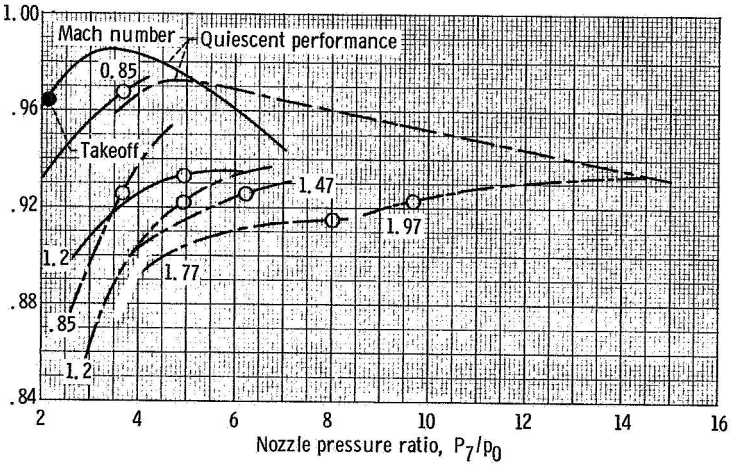

(c) Maximum-reheat.

Figure 14. - Performance of two-position shroud nozzle at assumed flight conditions.

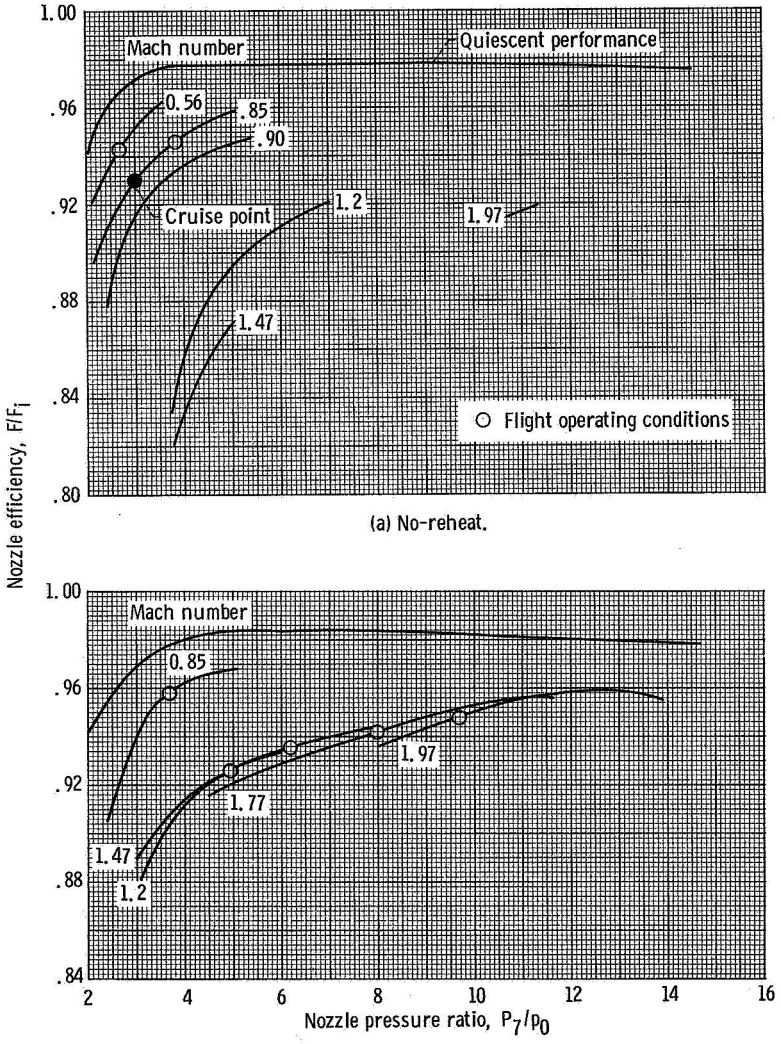

Figure 15. - Performance of floating shroud nozzle at assumed flight conditions.

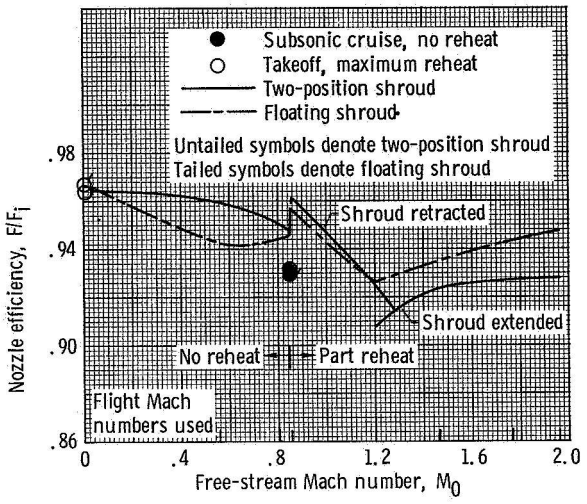

Figure 16. - Comparison of nozzle performance for two-position and floating shroud. Part reheat assumed for transonic acceleration.

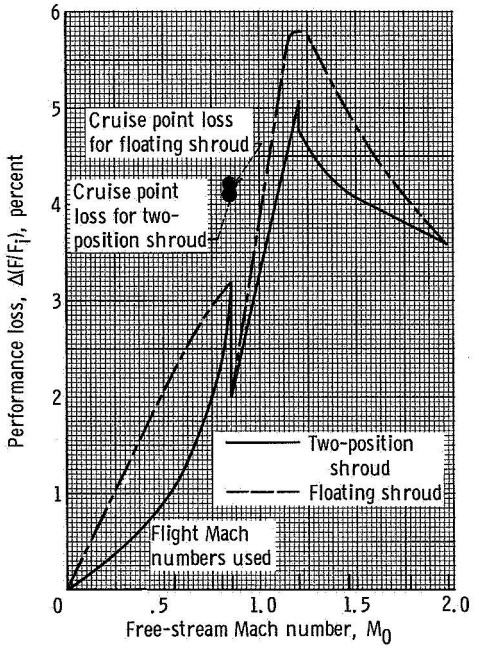

Figure 17. - Performance loss due to free-stream effects. Part reheat for transonic acceleration.

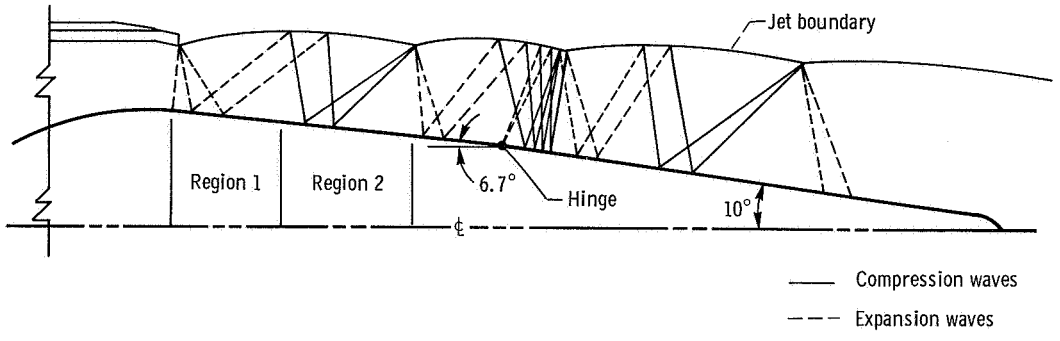

(a) Quiescent.

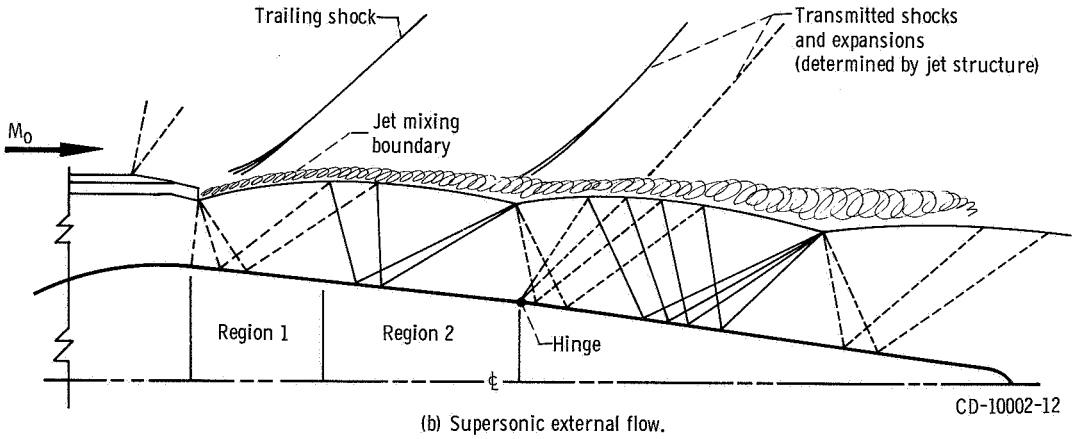

(b) Supersonic external flow.

Figure 18. - Flow field schematic for collapsible plug nozzle in part reheat configuration with shroud retracted. Nozzle pressure ratio greater than 2.0.

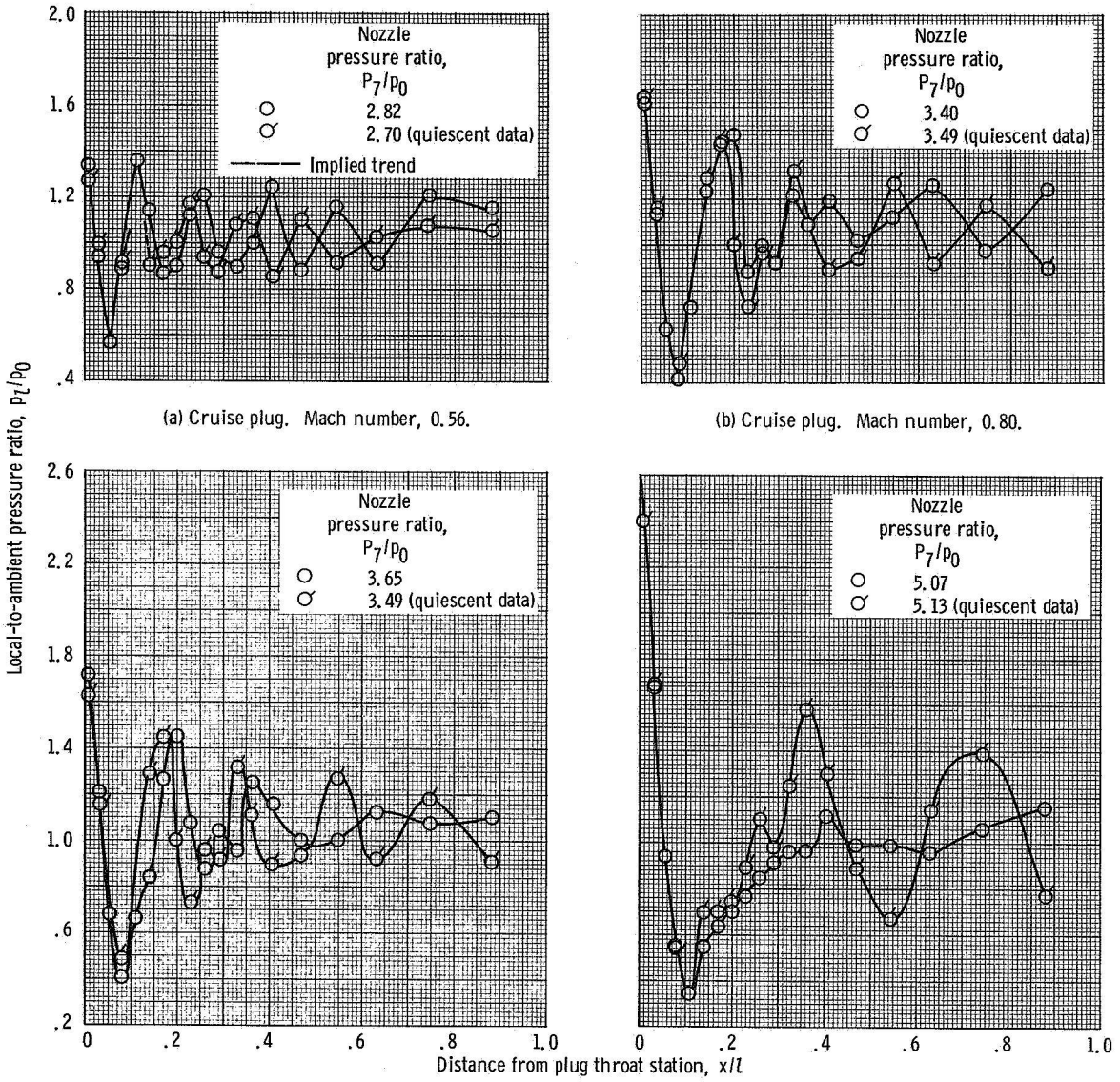

(a) Cruise plug. Mach number, 0.56.

(b) Cruise plug. Mach number, 0.80.

(c) Cruise plug. Mach number, 0.85.

(d) Cruise plug. Mach number, 1.2.

Figure 19. - Plug pressure distributions for two-position shroud nozzle, shroud retracted.

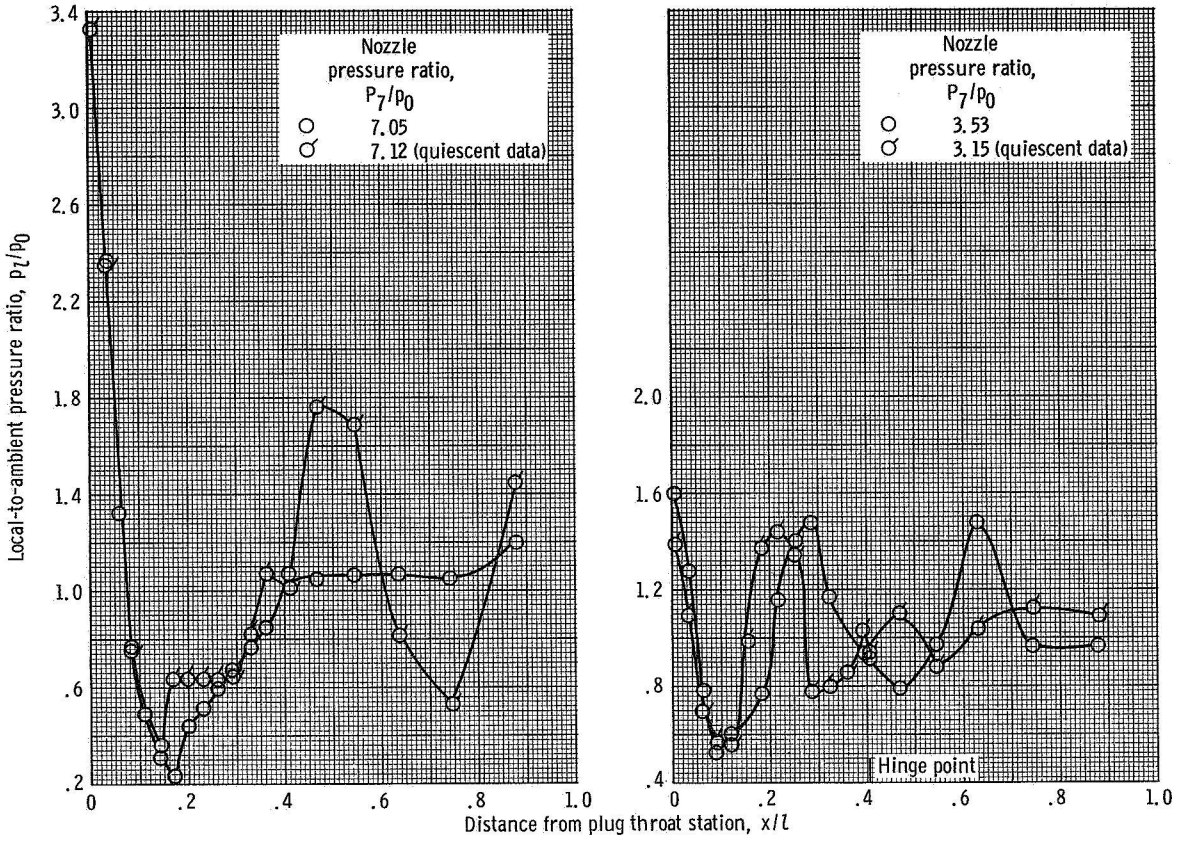

(e) Cruise plug. Mach number, 1.2.

(f) Part-reheat plug. Mach number, 0.85.

Figure 19. - Continued.

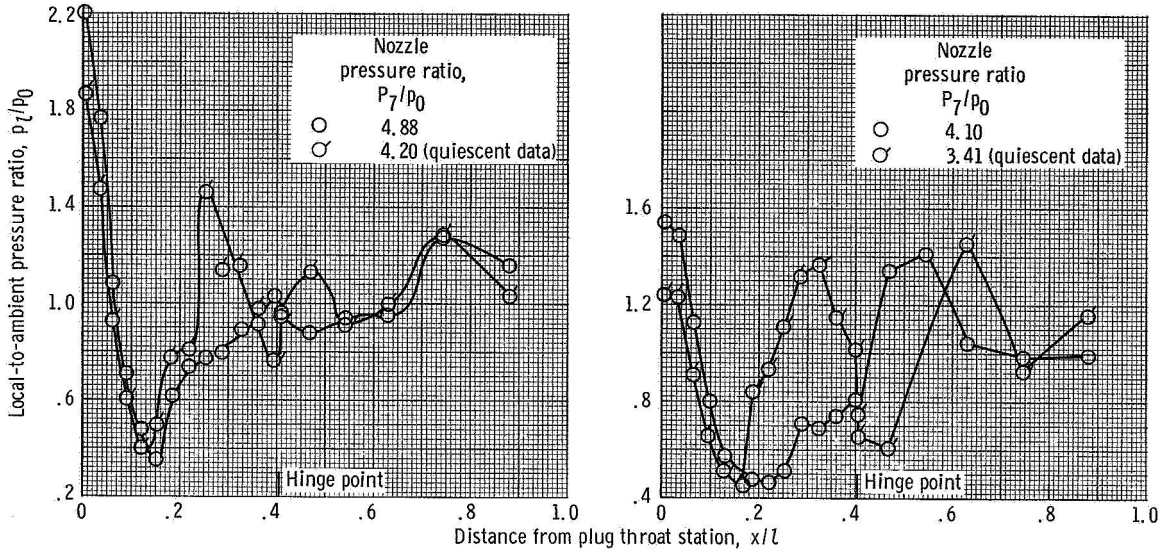

(g) Part-reheat plug. Mach number, 1.2.

(h) Maximum-reheat plug. Mach number, 0.85.

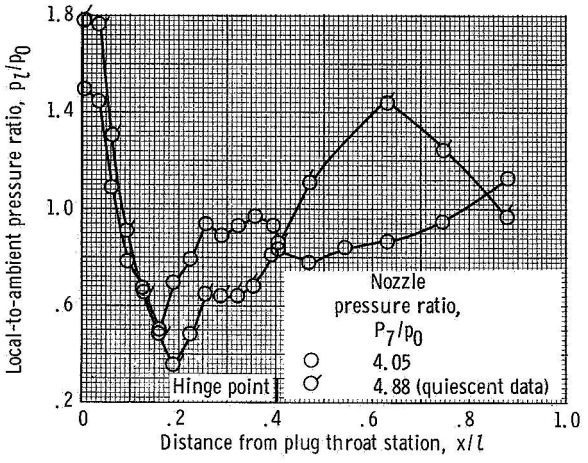

(i) Maximum-reheat plug. Mach number, 1.2.

Figure 19. - Concluded.

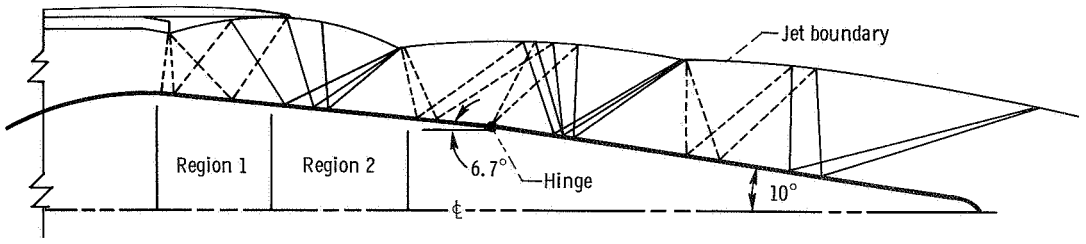

(a) Quiescent

——— Compression waves

– – – Expansion waves

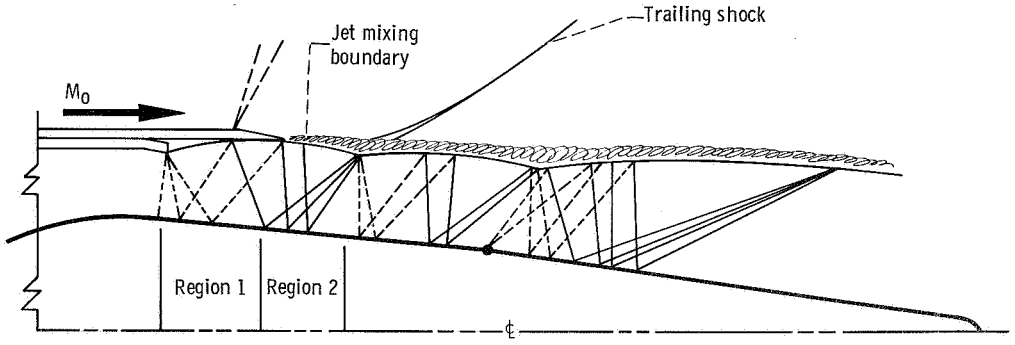

(b) Supersonic external flow.

CD-10003-12

Figure 20. - Flow field schematic for collapsible plug nozzle in part reheat configuration with shroud extended. Nozzle pressure ratio greater than 2.0.

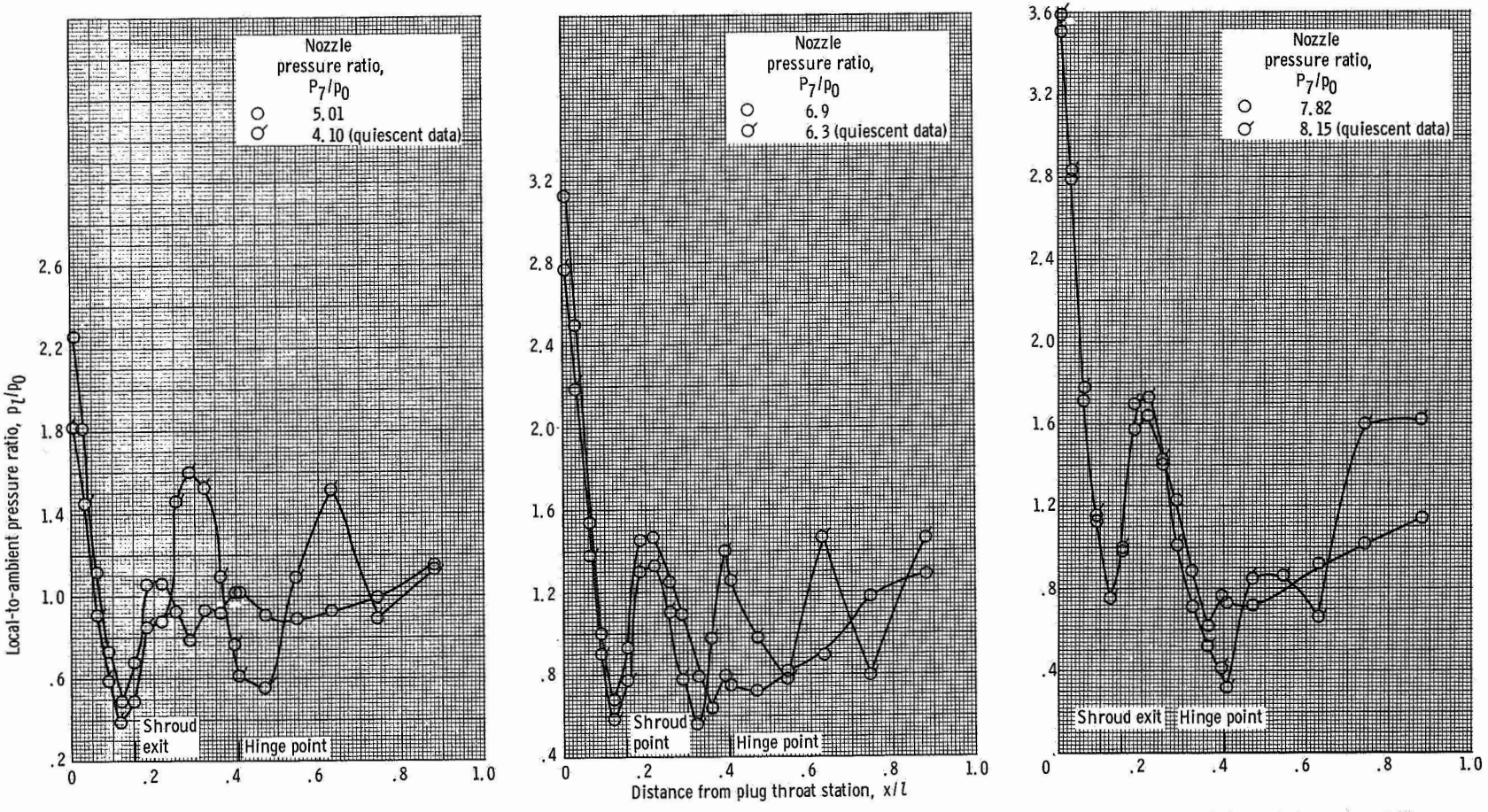

(a) Part-reheat plug. Mach number, 1.2.

(b) Part-reheat plug. Mach number, 1.47.

(c) Part-reheat plug. Mach number, 1.77.

Figure 21. - Plug pressure distributions for two-position shroud nozzle, shroud extended.

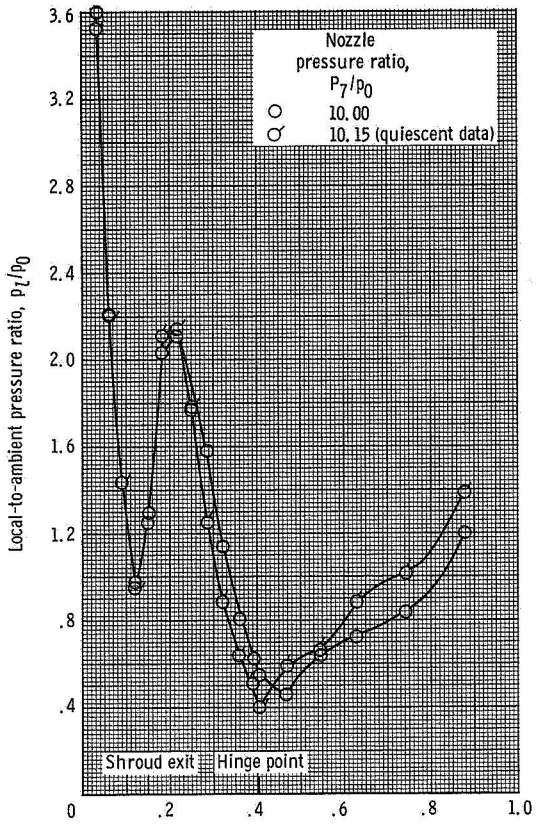

(d) Part-reheat plug. Mach number, 1.97.

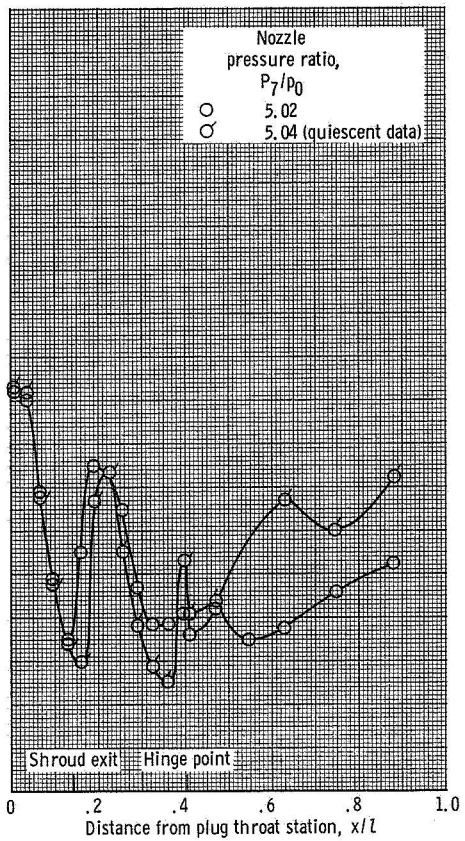

(e) Maximum-reheat plug. Mach number, 1.2.

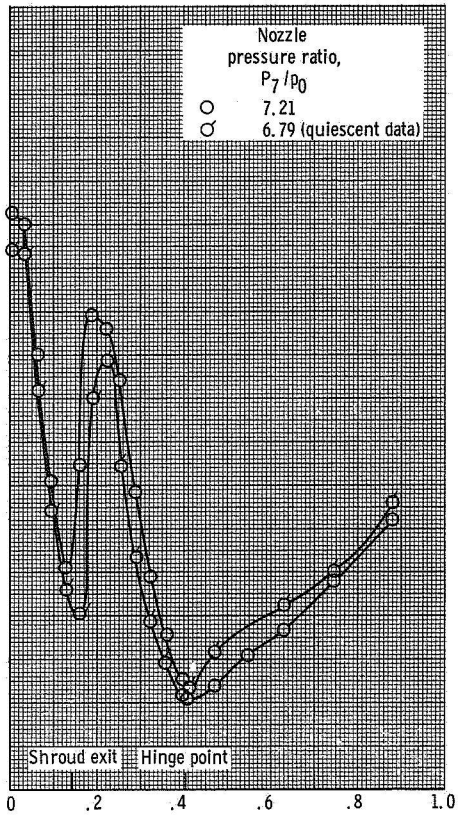

(f) Maximum-reheat plug. Mach number, 1.47.

Figure 21. - Continued.

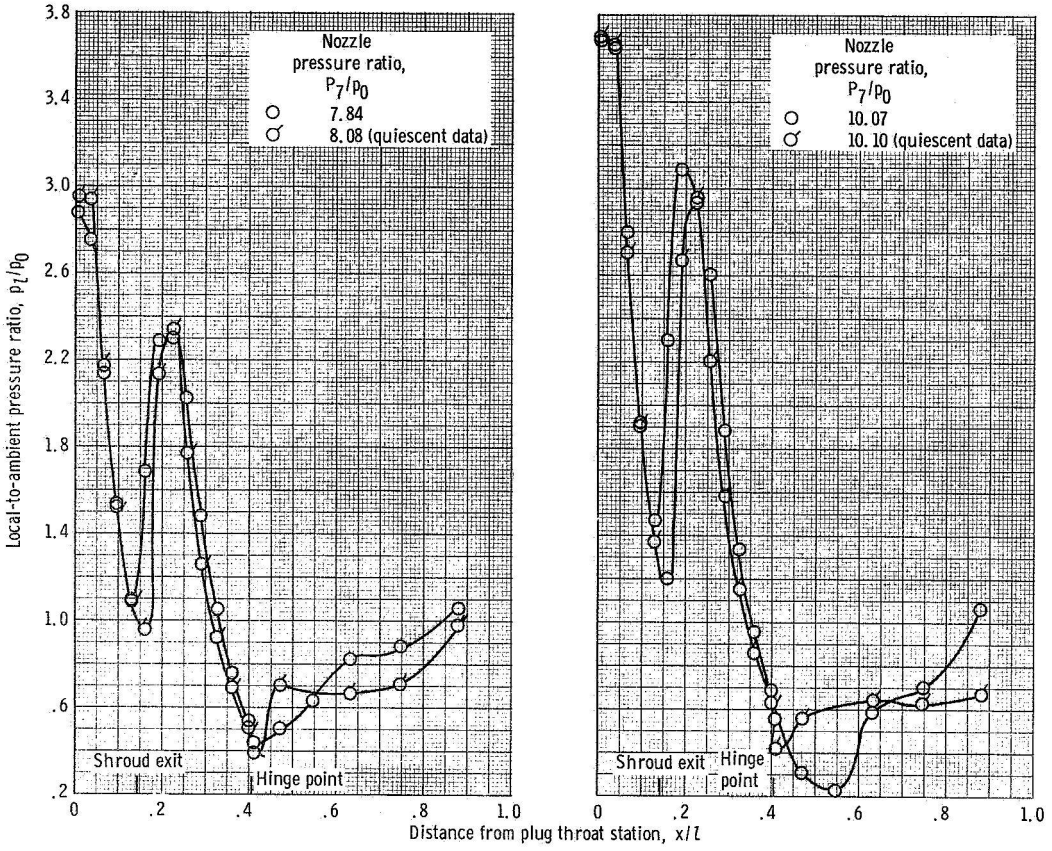

(g) Maximum-reheat plug. Mach number, 1.77.

(h) Maximum-reheat plug. Mach number, 1.97.

Figure 21. - Concluded.

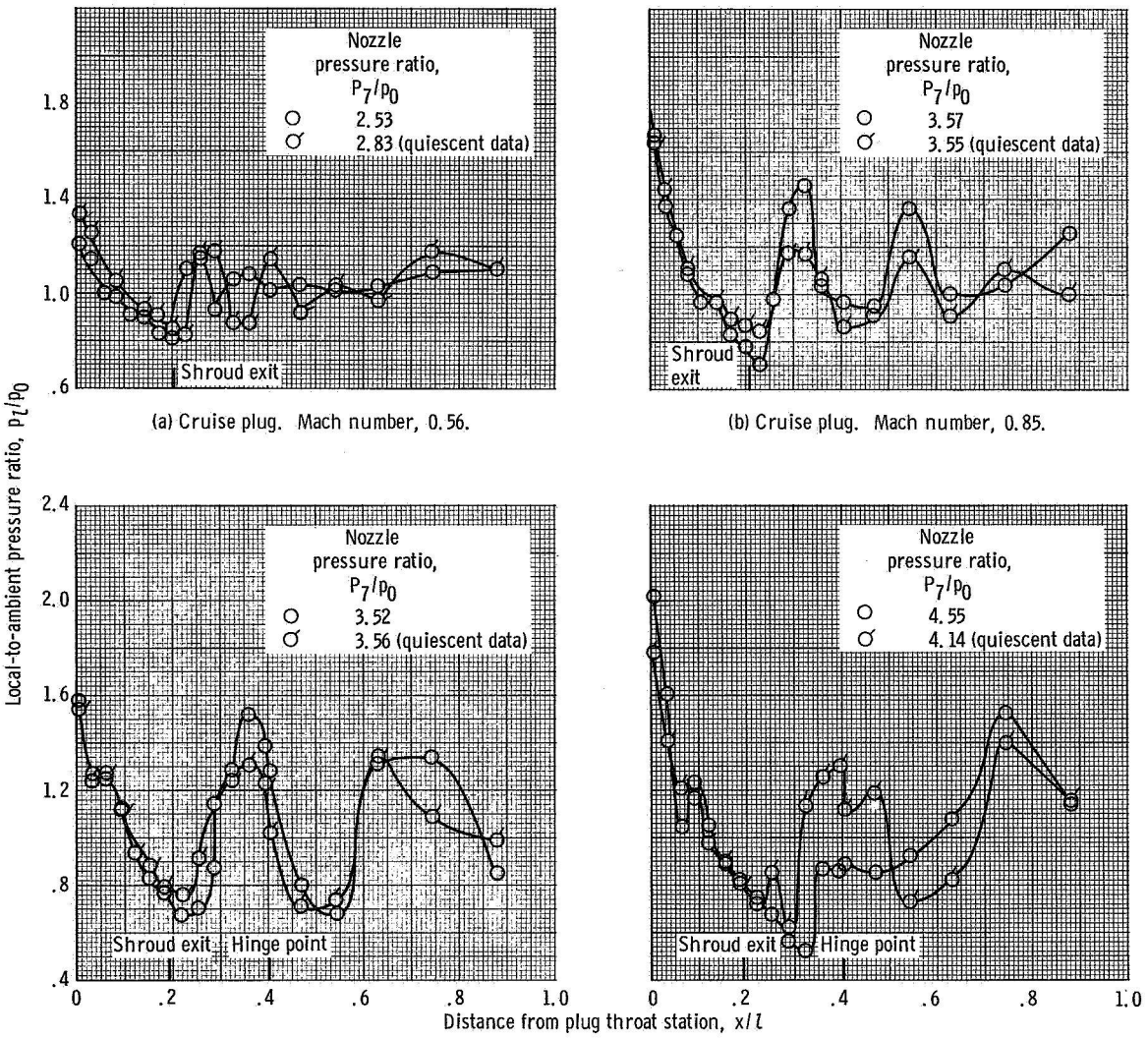

(a) Cruise plug. Mach number, 0.56.

(b) Cruise plug. Mach number, 0.85.

(c) Part-reheat plug. Mach number, 0.85.

(d) Part-reheat plug. Mach number, 1.2.

Figure 22. - Plug pressure distributions for floating shroud nozzle.

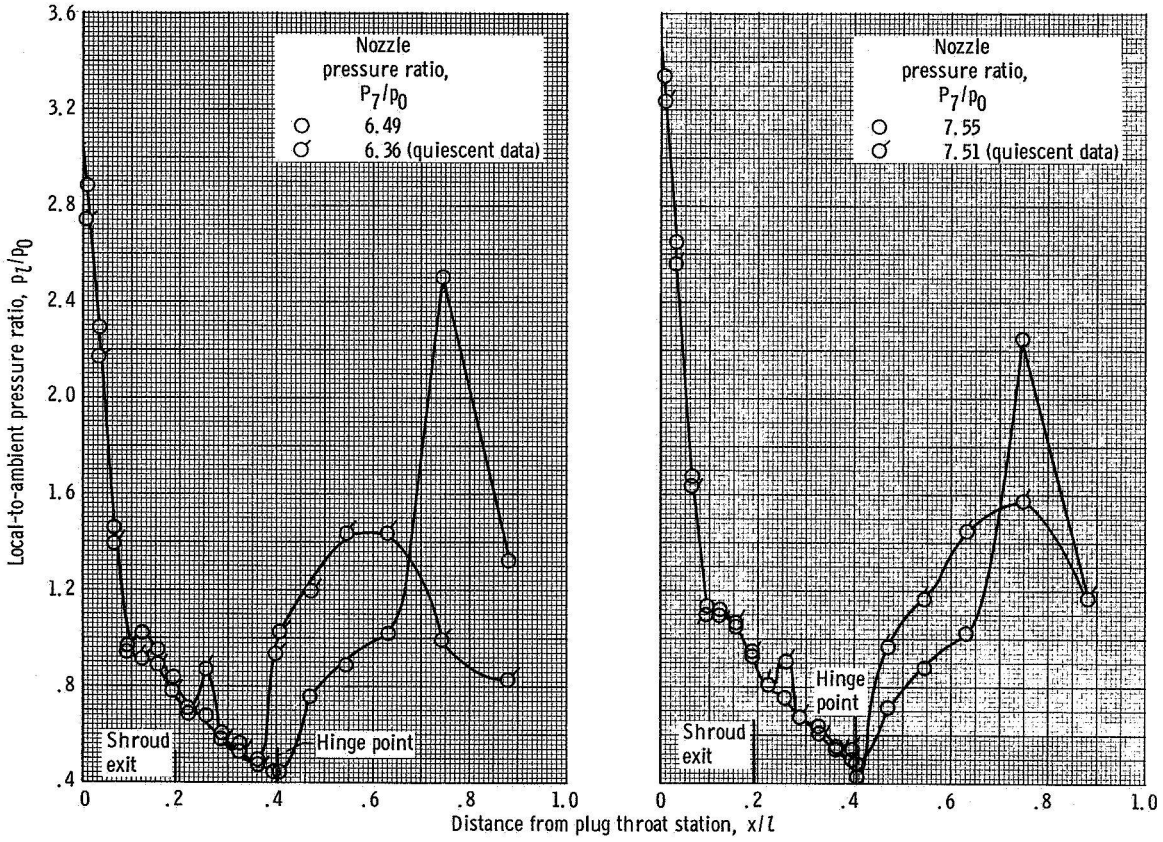

(e) Part-reheat plug. Mach number, 1.47.

(f) Part-reheat plug. Mach number, 1.77.

Figure 22. - Continued.

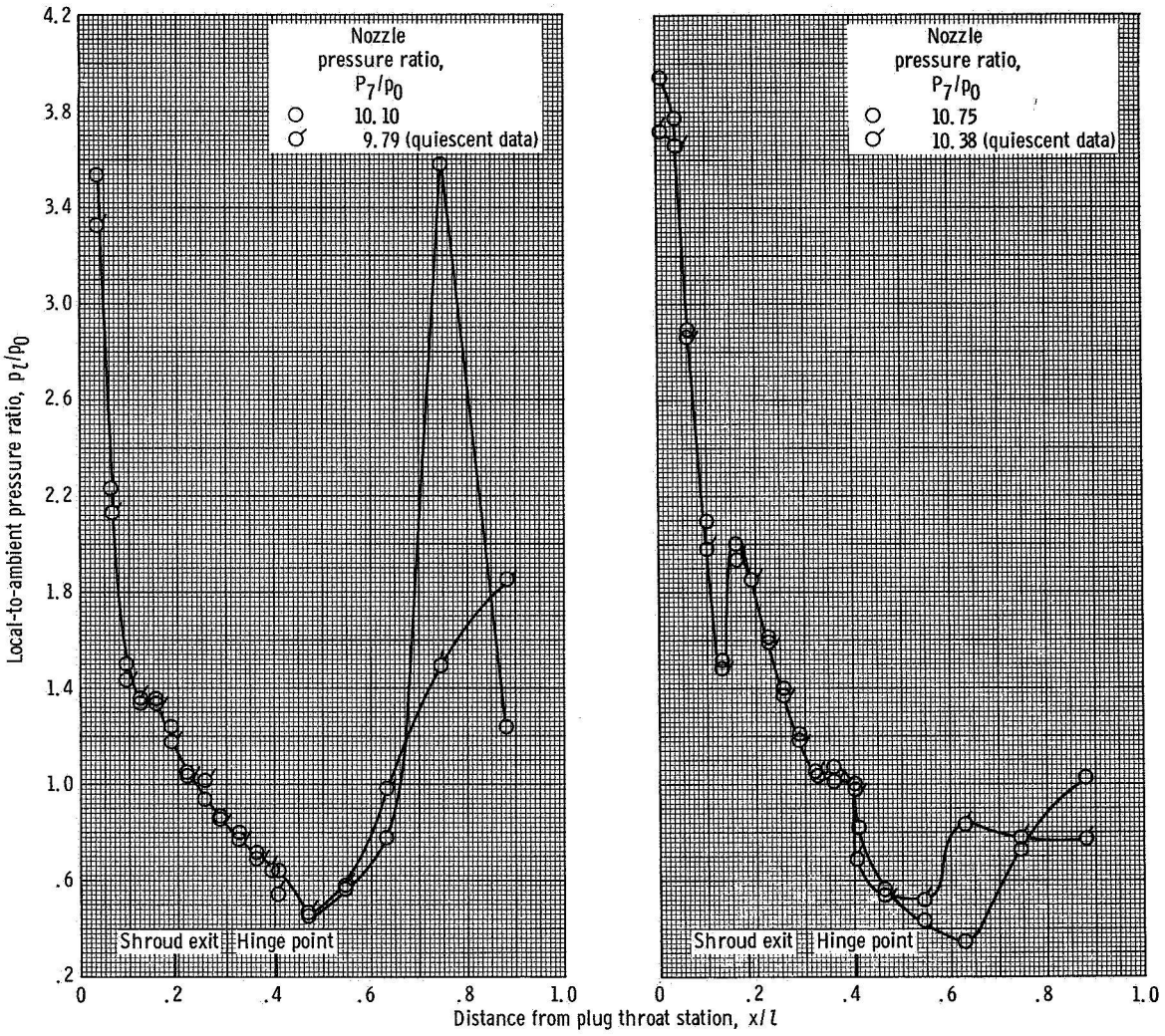

(g) Part-reheat plug. Mach number, 1.97.

(h) Maximum-reheat plug. Mach number, 1.97.

Figure 22. - Concluded.

"The aeronautical and space activities of the United States shall be conducted so as to contribute . . . to the expansion of human knowledge of phenomena in the atmosphere and space. The Administration shall provide for the widest practicable and appropriate dissemination of information concerning its activities and the results thereof."

—NATIONAL AERONAUTICS AND SPACE ACT OF 1958

NASA SCIENTIFIC AND TECHNICAL PUBLICATIONS

TECHNICAL REPORTS: Scientific and technical information considered important, complete, and a lasting contribution to existing knowledge.

TECHNICAL NOTES: Information less broad in scope but nevertheless of importance as a contribution to existing knowledge.

TECHNICAL MEMORANDUMS: Information receiving limited distribution because of preliminary data, security classification, or other reasons.

CONTRACTOR REPORTS: Scientific and technical information generated under a NASA contract or grant and considered an important contribution to existing knowledge.

TECHNICAL TRANSLATIONS: Information published in a foreign language considered to merit NASA distribution in English.

SPECIAL PUBLICATIONS: Information derived from or of value to NASA activities. Publications include conference proceedings, monographs, data compilations, handbooks, sourcebooks, and special bibliographies.

TECHNOLOGY UTILIZATION PUBLICATIONS: Information on technology used by NASA that may be of particular interest in commercial and other non-aerospace applications. Publications include Tech Briefs, Technology Utilization Reports and Notes, and Technology Surveys.

Details on the availability of these publications may be obtained from:

SCIENTIFIC AND TECHNICAL INFORMATION DIVISION

NATIONAL AERONAUTICS AND SPACE ADMINISTRATION

Washington, D.C. 20546